CELL BIOLOGY

A spatiotemporal Notch interaction map from plasma membrane to nucleus

Alexandre P. Martin[1], Gary A. Bradshaw[2], Robyn J. Eisert[1], Emily D. Egan[1], Lena Tveriakhina[1], Julia M. Rogers[1], Andrew N. Dates[1], Gustavo Scanavachi[3,4,5], Jon C. Aster[6], Tom Kirchhausen[3,4,5], Marian Kalocsay[7]*, Stephen C. Blacklow[1,8]†*

Notch signaling relies on ligand-induced proteolysis of the transmembrane receptor Notch to liberate a nuclear effector that drives cell fate decisions. Upon ligand binding, sequential cleavage of Notch by the transmembrane protease ADAM10 and the intracellular protease γ-secretase releases the Notch intracellular domain (NICD), which translocates to the nucleus and forms a complex that induces target gene transcription. To map the location and timing of the individual steps required for the proteolysis and movement of Notch from the plasma membrane to the nucleus, we used proximity labeling with quantitative, multiplexed mass spectrometry to monitor the interaction partners of endogenous NOTCH2 after ligand stimulation in the presence of a γ-secretase inhibitor and as a function of time after inhibitor removal. Our studies showed that γ-secretase–mediated cleavage of NOTCH2 occurred in an intracellular compartment and that formation of nuclear complexes and recruitment of chromatin-modifying enzymes occurred within 45 min of inhibitor washout. These findings provide a detailed spatiotemporal map tracking the path of Notch from the plasma membrane to the nucleus and identify signaling events that are potential targets for modulating Notch activity.

INTRODUCTION

Notch signaling is an essential and conserved mechanism of cell-cell communication that controls normal development and maintains adult tissue homeostasis in a wide range of tissues and organ systems (*1*, *2*). Mutations in Notch signaling components result in several human developmental disorders such as Alagille syndrome, caused by loss-of-function mutations affecting either the receptor NOTCH2 or the ligand JAGGED1 (*3*, *4*), spondylocostal dysostosis (*5*), and Hajdu-Cheney disease (*6*). In addition, Notch mutations and/or deregulated Notch signaling are frequently found in cancer (*7*). Activating mutations in *NOTCH1* occur in more than 50% of T cell acute lymphoblastic leukemias (T-ALL), and similar activating mutations have been found in triple-negative breast cancer, adenoid cystic carcinoma, and tumors derived from pericytes or smooth muscle (*7*). On the other hand, Notch acts as a tumor suppressor in cutaneous squamous cell carcinomas (*8*), highlighting the complexities in targeting Notch for cancer therapy.

Notch proteins (NOTCH1 to NOTCH4 in mammals) are transmembrane receptors that transmit signals in response to canonical Delta-like or Jagged ligands (DLL1, DLL4, JAG1, and JAG2) present on a signal-sending cell. Ligand binding initiates signal transduction by triggering a series of proteolytic cleavages of Notch in the receiver cell. The first ligand-induced cleavage is catalyzed by the metalloprotease ADAM10 at a site called S2, which is external to the plasma membrane, and generates a cleavage product referred to as the Notch extracellular truncation (NEXT). S2-cleaved Notch molecules are then cleaved by γ-secretase at site S3 in the transmembrane region near the inner membrane leaflet, resulting in the release of the Notch intracellular domain (NICD). NICD subsequently translocates into the nucleus and forms a Notch transcription complex with the DNA binding protein RBPJ and a MAML coactivator to induce the transcription of Notch target genes [see (*9*, *10*) for reviews].

Although these fundamental steps required for Notch signaling have been defined, it is less certain where γ-secretase cleavage takes place in the cell, whether NICD moves from membrane to nucleus by active or passive transport, and how long it takes NICD to migrate from membrane to nucleus after γ-secretase cleavage. Real-time luciferase complementation assays using ectopic expression of NOTCH1 and RBPJ fusion proteins have shown that immobilized ligand stimulation results in nuclear complementation between 30 and 60 min after removal of a γ-secretase inhibitor (GSI) (*11*), but analogous experiments have not been carried out at endogenous protein abundance. Previous reports have also reached different conclusions, for example, about whether γ-secretase cleavage occurs at the plasma membrane (*12*, *13*) or in an intracellular compartment (*14*–*16*).

To address these questions, we mapped the microenvironment of NICD and characterized its interactions with effectors within a native cellular environment in endogenous amounts after ligand stimulation in the presence of a GSI and then as a function of time after inhibitor removal. We used CRISPR-Cas9 genome editing in SVG-A cells, an astrocyte cell line, to fuse NOTCH2 to the engineered ascorbate peroxidase APEX2, which rapidly produces short-lived biotin-tyramide radicals that label proteins within a small radius (~20 nm) and that can be rapidly quenched (*17*–*19*).

[1]Department of Biological Chemistry and Molecular Pharmacology, Blavatnik Institute, Harvard Medical School, Boston, MA 02115, USA. [2]Department of Systems Biology, Laboratory of Systems Pharmacology, Harvard Medical School, Boston, MA 02115, USA. [3]Department of Cell Biology, Harvard Medical School, Boston, MA 02115, USA. [4]Program in Cellular and Molecular Medicine, Boston Children's Hospital, Boston, MA 02115, USA. [5]Department of Pediatrics, Harvard Medical School, Boston, MA 02115, USA. [6]Department of Pathology, Brigham and Women's Hospital, Boston, MA 02115, USA. [7]Department of Experimental Radiation Oncology, University of Texas MD Anderson Cancer Center, Houston, TX 77030, USA. [8]Department of Cancer Biology, Dana Farber Cancer Institute, Boston, MA 02215, USA.
*Corresponding author. Email: mkalocsay@mdanderson.org (M.K.); stephen_blacklow@hms.harvard.edu (S.C.B.)
†Lead contact.

We performed proximity labeling of the NOTCH2 microenvironment after ligand stimulation in the presence of a GSI and at different time points after inhibitor washout to identify changes in protein enrichment as a function of time by quantitative multiplexed proteomics. The dynamics of labeling enrichment of distinct plasma membrane, cytosolic, and nuclear proteins defined the microenvironment of NOTCH2-APEX2 during its passage from the plasma membrane to the nucleus. Our studies showed that γ-secretase cleavage of NOTCH2 to produce NICD2 occurred in an intracellular compartment, that passage of NICD2 through the cytoplasm was associated with transient proximities to membrane cortical and cytoskeletal proteins, and that formation of nuclear complexes and recruitment of chromatin-modifying enzymes occurred within 45 min of GSI washout. This work provides a detailed spatiotemporal map tracking the itinerary of Notch from membrane to nucleus after metalloprotease cleavage and identifies events in signal transmission that are potential targets for modulating Notch activity.

RESULTS

System validation and genome engineering for NOTCH2 proximity labeling in SVG-A cells

To track the movement of Notch as a function of time in response to signal induction, we labeled proteins in the Notch microenvironment using a NOTCH2-APEX2 ascorbate peroxidase fusion protein (*20*–*22*). We investigated the response associated with the NOTCH2-JAG1 receptor-ligand pair because this pairing transmits signals that are required for normal development (*1*), as highlighted by Alagille syndrome, a multiorgan disorder caused by loss-of-function mutations in either *NOTCH2* or *JAGGED1* (*3*, *4*). To achieve the precise synchronization necessary for time-resolved proximity labeling, we used immobilized JAG1 as an activating ligand in concert with a potent, specific GSI, the effects of which can be rapidly reversed by simple washout (*23*). We selected SVG-A human fetal astrocytes as our receptor-expressing cells ("Notch" or "receiver" cells) because they produce abundant NOTCH2 endogenously and only very low amounts of the other Notch receptors (fig. S1A). We confirmed that NOTCH2 was responsible for the Notch transcriptional response in these cells by knocking out NOTCH2 using CRISPR/Cas9 genome editing (*24*): The absence of NOTCH2 effectively abolished Notch reporter gene activity in a signaling assay using immobilized JAG1 as ligand (fig. S1, B and C), confirming both that these cells were responsive to JAG1 and that the reporter signal in these cells was a consequence of NOTCH2 activation.

To ensure that our studies were performed at natural receptor abundance, we used CRISPR/Cas9 to add APEX2 and hemagglutinin (HA) coding sequences to the 3′ end of *NOTCH2*, creating a fusion gene at the endogenous locus encoding NOTCH2 fused to APEX2-HA at its C terminus (fig. S1D). The cassette for homologous recombination also contained a T2A sequence followed by a sequence encoding the mNeonGreen fluorescent protein, allowing us to isolate single cells positive for the desired genomic insertion by fluorescence-activated cell sorting (FACS). We confirmed that the NOTCH2-APEX2-HA fusion protein matured similarly to wild-type NOTCH2 in parental cells (fig. S1E), was present in similar amounts on the cell surface (fig. S1, F and G), retained signaling activity in response to immobilized JAG1 comparable to wild-type NOTCH2 in a reporter gene assay, and was silenced similarly to wild-type NOTCH2 by inhibitors of ADAM10 and γ-secretase cleavage (fig. S1H). Western blot analysis also confirmed that biotinylation of proteins across a wide range of molecular weights was only observed in cells carrying the APEX2 fusion protein (fig. S1I).

Time-resolved NOTCH2 proximity labeling with the APEX2 fusion protein

Because soluble ligands do not activate Notch, it is not possible to use acute addition of the ligand to initiate the signal. To try to mimic an acute initiation event, we attempted to use the removal of a selective ADAM10 inhibitor, GI254023X (GI25X) (*25*), to serve as the event initiating S2 cleavage induced by immobilized ligand. If this approach were successful, it would have also allowed us to track dynamic events beginning with the S2 cleavage step generating the NEXT fragment. Unfortunately, however, this approach suffered from two complications that precluded the acquisition of time-resolved proteomic information about signaling. First, "leaky" NOTCH2 proteolysis still occurred in the presence of the inhibitor, likely because ADAM17 or another protease can substitute for ADAM10 in catalyzing S2 cleavage to generate the NEXT fragment. Second, the synchronization of events was poorer when this inhibitor was used (fig. S2A), and as a result, it was necessary to use removal of a GSI to achieve the temporal resolution required for dynamic analysis of the Notch molecular neighborhood.

We thus cultured NOTCH2-APEX2-HA knockin cells on culture plates containing immobilized JAG1 (*26*–*28*) overnight (16 hours) in the presence of the GSI Compound E and analyzed protein biotinylation as a function of time after GSI removal by mass spectrometry (MS) (Fig. 1, A and B). We used a condition without ligand to serve as a baseline to define the molecular neighborhood of NOTCH2 in the absence of ligand. For the other conditions, we incubated the cells on immobilized ligand in the presence of GSI, set the time of inhibitor removal (when the medium containing GSI was replaced with a GSI-free medium) to $t = 0$, and followed the time course of the NOTCH2 molecular neighborhood as a function of time after GSI washout (Fig. 1B). The cells were never treated with trypsin or EDTA, nor were they ever detached from the plate or resuspended, because all of these manipulations can activate Notch. We confirmed that GSI washout resulted in accumulation of NICD2 over a 2-hour time course (fig. S2B), performed proximity labeling using biotin phenol and hydrogen peroxide at various time points up to 2 hours, and by Western blot observed specific labeling of cohorts of biotin-labeled proteins that changed with time (fig. S2C).

MS analysis of biotinylated proteins labeled by NOTCH2-APEX2 (fig. S3A) determined the temporal profiles of labeling for 980 proteins that displayed different dynamic labeling patterns after Notch activation. The high correlation between replicates (fig. S3B) and the clustering of replicates in principal components analysis (fig. S3C) attested to the reproducibility of our experimental system. When referenced to the $t = 0$ time point, the transcriptional coactivator MAML1, an essential component of the Notch transcriptional complex (*29*, *30*), was not significantly enriched at early time points after GSI washout (<30 min) but became the most significantly enriched protein 2 hours after GSI washout (see below), a finding independently verified by Western blot (fig. S3D). This observation confirmed nuclear translocation of NICD2 after GSI removal and highlighted the dynamic nature of the NICD2

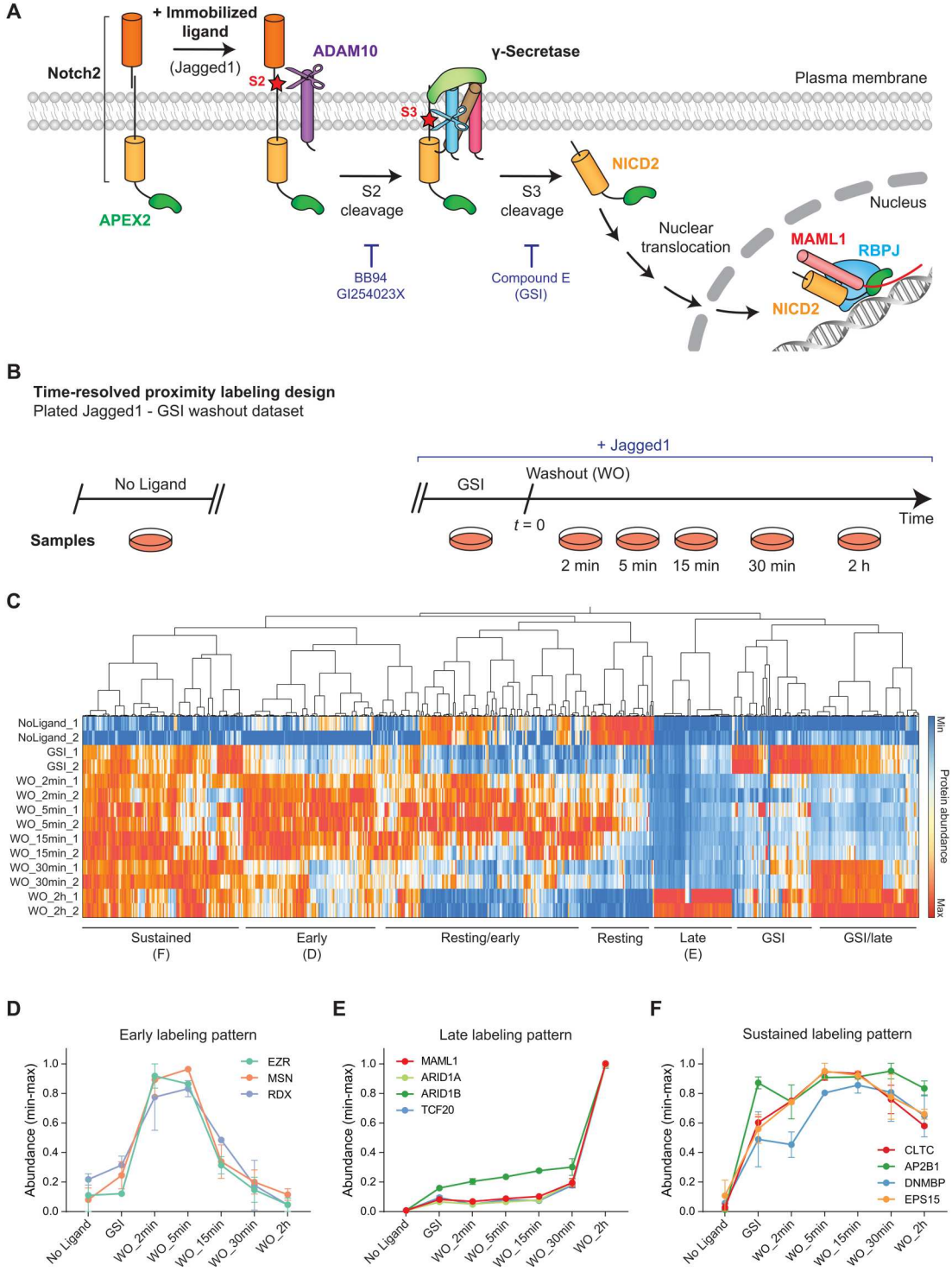

Fig. 1. Design, experimental procedure, and overall kinetic profiles of time-resolved NOTCH2-APEX2 proximity labeling in SVG-A cells. (**A**) Schematic of key steps in NOTCH2 signaling induced by immobilized JAG1 ligand. JAG1 stimulates NOTCH2 proteolysis at S2 by ADAM10, followed by γ-secretase cleavage at S3. The S3-cleaved NOTCH2 intracellular domain (NICD2) transits to the nucleus and associates with RBPJ and the transcriptional coactivator MAML1 to induce the expression of target genes. BB94 and GI254023X (also referred as GI25X) are inhibitors of ADAM10, and Compound E (referred to as GSI) is a potent inhibitor of γ-secretase. (**B**) Schematic showing the design for time-resolved proximity labeling by NOTCH2-APEX2 using immobilized JAG1 as ligand and washout of GSI at time $t = 0$. (**C**) Heatmap of hierarchical clustering of NOTCH2-APEX2 proximity labeling as a function of time after GSI washout (WO). Clustering of the relative abundance of each identified protein (columns) as a function of time (rows) was performed using Ward's minimum variance method. (**D** to **F**) Kinetic profiles of representative proteins showing an early (D), late (E), or sustained (F) labeling pattern. Data in (C) to (F) are from simultaneous MS analysis of 14 samples from one labeling time course ($n = 1$), with two technical replicates analyzed for each time point.

microenvironment as a function of time. We also note that our MS workflow did not identify all known Notch-associated proteins in this study, likely because MS proteomics often does not capture all protein analytes present. For example, RBPJ, the transcription factor bound by NICD in the transcriptional activation complex, was not detected, although RBPJ was biotinylated as early as 30 min after GSI washout with a peak of relative abundance at 2 hours after washout, as judged by Western blot (fig. S3E).

Hierarchical clustering of the relative abundance of each labeled protein as a function of time (data file S1) led to the identification of seven distinct patterns of enrichment based on Ward's hierarchical clustering method (Fig. 1C). These seven clusters showed maximum labeling: (i) in the absence of ligand; (ii) with ligand in the presence of GSI; (iii) early (2 to 5 min) in the washout time course (Fig. 1D); (iv) 2 hours after washout (Fig. 1E); (v) throughout the time course in the presence of ligand, but not when ligand is absent (Fig. 1F); (vi) with ligand in the presence of GSI and at later time points; and (vii) both in the absence of ligand and at early time points.

To investigate whether JAG1 stimulation in a cellular context affected the dynamics of NICD2 interactions, we also cocultured JAG1-expressing A673 sarcoma cells with NOTCH2-expressing cells in the presence of GSI followed by inhibitor washout. The presence of ligand-expressing cells, however, led to increased noise in studies spanning two different time windows (fig. S4, A to C). The trends seen in the datasets from these efforts (data files S2 and S3) were fully consistent with the results of the GSI washout using immobilized ligand, but the signals were much noisier and incomplete (fig. S5, A to E). MAML1 was not detected at the 2-hour time point, for example, in the coculture experiments. The use of immobilized ligand was the only approach that eliminated interference from ligand-expressing cells, a decision necessary to achieve sufficient signal-to-noise for a robust time-resolved analysis.

NOTCH2 is internalized after S2 but before S3 cleavage

Not surprisingly, the first cluster, which exhibited maximum labeling enrichment in the absence of immobilized ligand (Fig. 1C), was characterized by proteins that reside at the plasma membrane (Fig. 2, A and B), where Notch encounters its transmembrane ligands present on neighboring cells. This group of proteins included EGFR (epidermal growth factor receptor), the folate carrier SLC19A1, ERBIN (erbin), GPRC5A (retinoic acid–induced protein 3), DBN1 (drebrin), and surface-associated proteins such as the catenins CTNNB1 and CTNND1.

In the presence of GSI, ligand binding induces metalloprotease cleavage, but γ-secretase–catalyzed cleavage at S3 is blocked, preventing liberation of NICD2 from the membrane. When GSI was present, plasma membrane–associated proteins, which were enriched in the first cluster when ligand was not present, become depleted as compared with unstimulated cells (Fig. 2C). Instead, proteins that exhibited maximal enrichment in their proximity to NOTCH2 after ligand exposure in the presence of GSI were predominantly associated with vesicular or endosomal compartments and the endocytic machinery (Fig. 2, C to E). Core components participating in clathrin-mediated endocytosis (CME), including clathrin, AP-2, dynamin, and EPS15, were enriched (Figs. 1F and 2D), as was the transferrin receptor, which enters cells through CME, and other proteins implicated in vesicular trafficking, such as EHD1, SEC22B, and SNX3 (Fig. 2, C to E). In addition, there was a substantial enrichment of vesicle-associated TMED (transmembrane emp24 domain) proteins upon ligand stimulation (Fig. 2, C and D), specifically TMEM165 and TMEM43. The vesicle-associated proteins VAPA and VAPB (*31*, *32*) also showed maximum enrichment in the presence of GSI (Fig. 2D). Another group of proteins showed labeling enrichment in the presence of GSI that persisted after washout (Fig. 2D). This group included proteins related to endocytosis and vesicular trafficking (Fig. 2E), as well as the β-amyloid precursor protein (APP; Fig. 2D), a well-known substrate of the γ-secretase complex (*33*). Last, proteins related to endocytosis and components of the CME machinery (Fig. 2D) exhibited a significant increase in abundance upon ligand stimulation, with variable enrichment after GSI washout (Figs. 1F and 2D).

The comparison between the no-ligand and GSI conditions suggested that NOTCH2 underwent internalization after ligand-induced ADAM10 cleavage at site S2. To evaluate this possibility using a complementary approach, we used NOTCH2-Halo knockin SVG-A cells, in which a HaloTag was inserted at the endogenous NOTCH2 locus after the C-terminal A2471 residue using CRISPR-Cas9. We monitored the subcellular localization of NOTCH2 by immunofluorescence after washout of GI25X, a potent ADAM10 inhibitor (*25*), in the absence or presence of the dynamin inhibitor hydroxy-dynasore, which blocks endocytosis (*34*–*36*). Cells were incubated overnight on immobilized JAG1 in the presence of GI25X, after which the inhibitor was removed to allow S2 cleavage of ligand-bound NOTCH2 in the absence or presence of hydroxy-dynasore. As anticipated, washout of GI25X in the absence of the dynamin inhibitor resulted in nuclear accumulation of NICD2 by 2 hours after washout (Fig. 3, A to C), indicating that S2 cleavage, S3 cleavage, and nuclear translocation had occurred. However, washout of GI25X in the presence of hydroxy-dynasore significantly impaired the nuclear accumulation of NICD2 (Fig. 3, A to C). In addition, the inhibition of endosomal acidification by bafilomycin A1 (BafA1), a specific vacuolar H^+–adenosine triphosphatase (ATPase) inhibitor (*37*–*39*), or by chloroquine (*40*) also impaired NOTCH2 nuclear accumulation after GI25X washout (Fig. 3, A to C), further suggesting that S3 cleavage required access to an acidified intracellular compartment. None of these inhibitors significantly modified the subcellular localization of unstimulated NOTCH2 (fig. S6A), consistent with the conclusion that they act after ligand-induced S2 cleavage of NOTCH2.

The generation of the S3-cleaved form of NOTCH2 (NICD2) after GI25X washout was also evaluated by Western blotting using an antibody that specifically recognizes the N-terminal epitope of NICD2 (*41*). As expected, washout of GI25X resulted in an increase in NICD2 abundance that was also greatly impaired by the inhibition of endocytosis or vesicular acidification (Fig. 3, D and E). Last, the effect of inhibiting endocytosis or vesicular acidification on Notch transcriptional activity was investigated using a well-characterized luciferase reporter assay (*29*, *42*, *43*). Washout of GI25X induced a Notch-dependent transcriptional response that was substantially reduced by the presence of hydroxy-dynasore, BafA1, or chloroquine (Fig. 3F). In contrast, however, when GSI was washed out, NICD2 accumulated in the nucleus after 2 hours, independent of whether an endocytosis or acidification inhibitor was present (Fig. 3, G and H, and fig. S6B), placing the step requiring endocytosis between S2 and S3 cleavage. This sensitivity extended to other members of the Notch receptor family, because NICD1

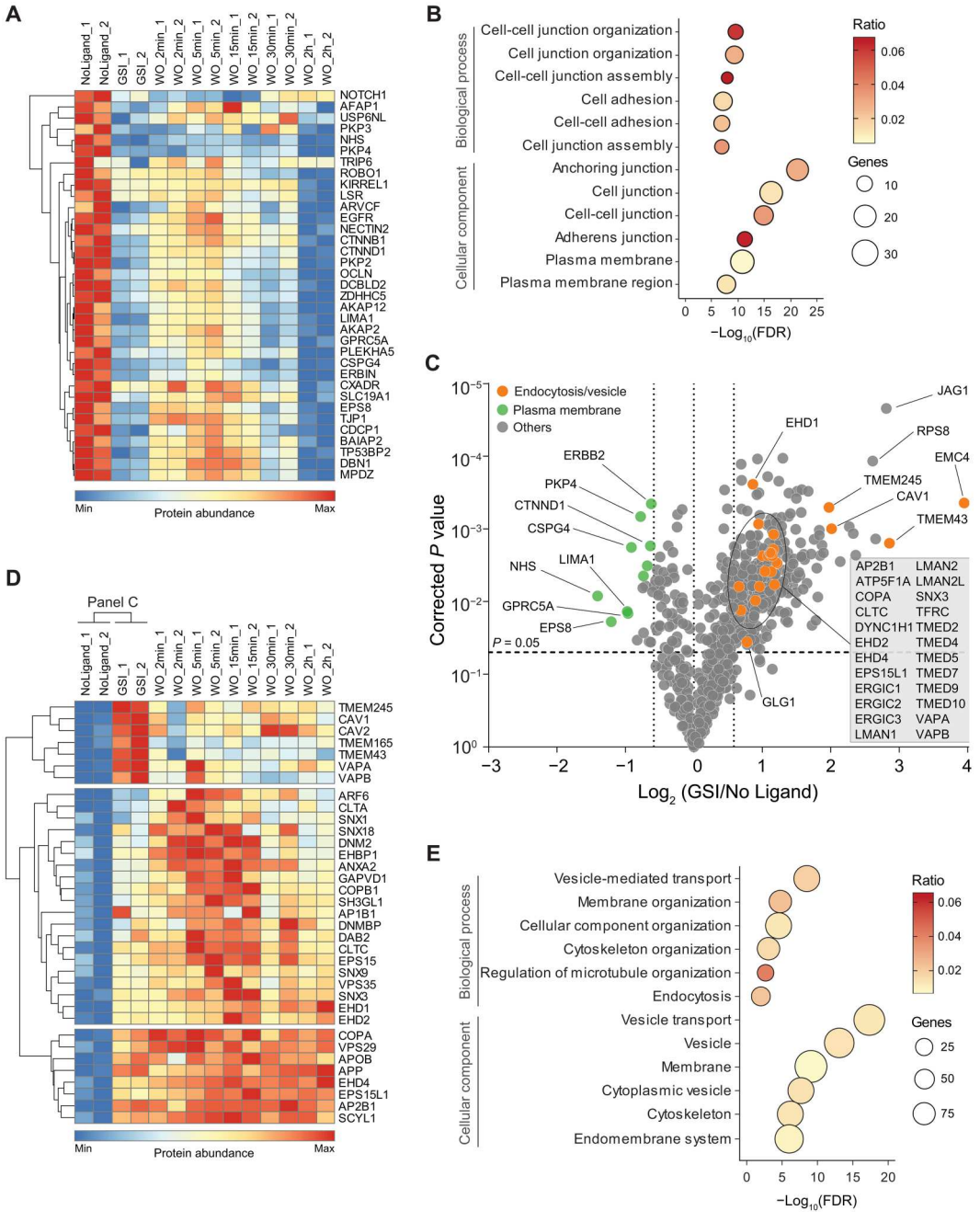

Fig. 2. The NOTCH2 molecular neighborhood changes dynamically as a function of time after ligand stimulation. (**A**) Heatmap of hierarchical clustering of proteins characterized by peak relative abundance in conditions without Notch stimulation by ligand. (**B**) Gene Ontology terms for proteins significantly enriched in (A). (**C**) Volcano plot comparing the relative abundance of proteins enriched upon JAG1 stimulation in GSI compared with no ligand stimulation. Significantly enriched proteins [$P \leq 0.05$, fold change (FC) ≥ 1.5] related to endocytosis and/or vesicular-mediated transport are labeled in orange, whereas significantly reduced proteins that localize to the plasma membrane are labeled in green. *P* values are Benjamini-Hochberg–corrected. (**D**) Heatmap focused on proteins related to endocytosis and vesicular transport identified in the time-resolved NOTCH2-APEX2 proximity labeling analysis. (**E**) Gene Ontology terms for proteins significantly enriched in (C) and (D). Data in all panels are from simultaneous MS analysis of 14 samples from one labeling time course ($n = 1$), with two technical replicates analyzed for each time point.

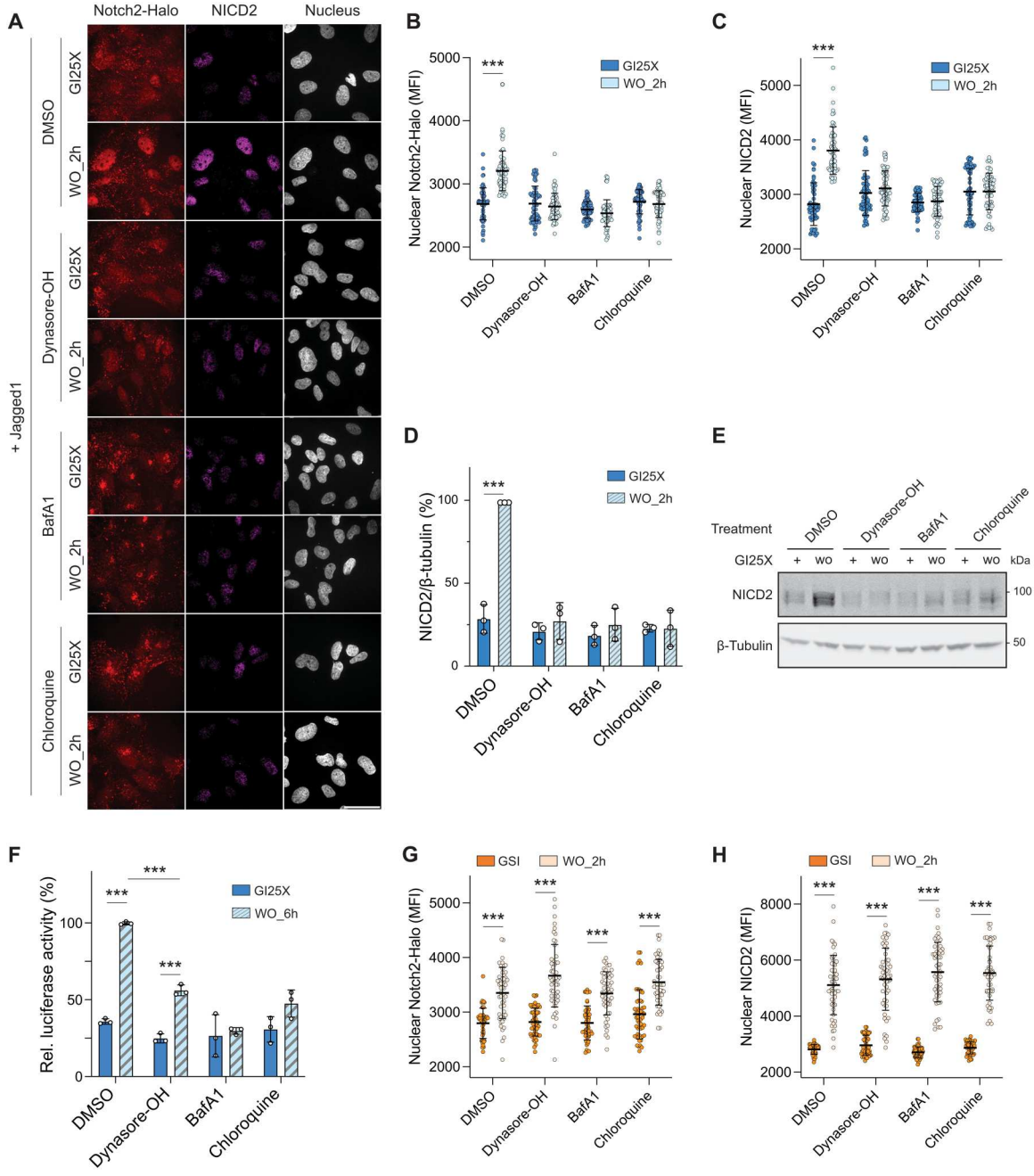

Fig. 3. NOTCH2 is internalized after S2 cleavage and accesses an acidified intracellular compartment. (**A**) Representative images of JAG1-stimulated SVG-A NOTCH2-HaloTag cells showing the cellular distribution of NOTCH2-HaloTag (NOTCH2-Halo) and S3-cleaved NICD2 after removal of the ADAM10 inhibitor GI25X in the absence or presence of hydroxy-dynasore (dynasore-OH), bafilomycin A1 (BafA1), or chloroquine. The HaloTag was labeled with JaneliaFluorX549 HaloTag ligand, and NICD2 was stained with an antibody recognizing NICD2. Nuclei were identified by DAPI staining. Scale bar, 20 μm. (**B** and **C**) Quantification of mean fluorescence intensity (MFI) in the nucleus for NOTCH2-Halo (B) and for NICD2 (C) for the imaging data presented in (A) for a total of 90 cells. (**D**) Quantification of Western blot data for NICD2 abundance in parental SVG-A cells after GI25X washout in the presence of dynasore-OH, BafA1, or chloroquine. (**E**) Representative Western blot for NICD2 quantified in (D). (**F**) Notch luciferase reporter assay. Parental SVG-A cells were stimulated by immobilized JAG1 overnight in the presence of GI25X, and the relative luciferase activity was measured 6 hours after removal of the ADAM10 inhibitor GI25X in the absence or presence of dynasore-OH, BafA1, or chloroquine. β-Tubulin is a loading control. (**G** and **H**) Quantification of MFI in the nucleus (images in fig. S6B) for NOTCH2-Halo (G) and activated NICD2 (H) after removal of the GSI Compound E in the absence or presence of dynasore-OH, BafA1, or chloroquine for a total of 90 cells. All data presented in this figure are from three independent experiments ($n = 3$) and are presented as mean ± SD. *$P \leq 0.05$, *$P \leq 0.01$, and ***$P \leq 0.001$. Two-way ANOVA followed by Tukey's pairwise comparison was used for statistical comparisons.

generation was also reduced in SVG-A cells upon the inhibition of endocytosis or vesicular acidification after GI25X washout (fig. S7A). Moreover, this sensitivity was cell line–independent, because inhibitors of endocytosis or vesicular acidification reduced the generation of both NICD1 and NICD2 in 293T cells (fig. S7B), U2OS cells (fig. S7C), HeLa cells (fig. S7D), and U251 cells (fig. S7E). These results argue that bound ligand induces metalloprotease cleavage at S2 at the cell surface and that the S2-cleaved form of NOTCH2 is then internalized to an intracellular compartment where it is cleaved by γ-secretase, thereby allowing NICD2 to access the nucleus.

NICD2 is not actively transported through the cytosol

In our dataset, we identified a class of proteins for which the relative abundance increased shortly after GSI washout (2 to 5 min) (Fig. 1, C and D). Among the proteins in this cluster, we detected the ERM proteins ezrin (EZR), radixin (RDX), and moesin (MSN), which play a role in linking membranes to the actin cytoskeleton (Fig. 4, A and B) (*44*, *45*). In addition to their architectural role, ERM proteins have been implicated in the maturation of endosomes and trafficking of EGFR (*46*). These results indicate that a pool of NICD2 molecules relocates to an ERM-enriched microenvironment upon or immediately after γ-secretase cleavage to generate NICD2.

To examine whether the activity of ERM proteins modulates NOTCH2 signaling in these cells, we treated NOTCH2-Halo knockin SVG-A cells either with control small interfering RNA (siRNA) (siCtrl) or with a mixture of siRNAs that suppressed the expression of all three ERM proteins simultaneously (fig. S8, A and B) and activated signaling by GSI washout after culturing on immobilized JAG1. Both control-treated cells and cells treated with the ERM siRNA mixture exhibited a comparable increase in the amount of nuclear NICD2 2 hours after washout (fig. S8, C and D). Likewise, control-treated cells and cells treated with the ERM siRNA mixture exhibited similar increases in the amount of NICD2 detectable by Western blot (fig. S8, E to H), and there was no significant difference between the two treatments when the induction of reporter gene activity was measured after GSI removal (fig. S8, I to K). In a complementary experiment, we also tested whether treatment with a dominant-negative form of Ezrin (*47*, *48*) affected nuclear accumulation of NICD2 and again did not observe a substantial difference among the vehicle-treated, wild-type Ezrin–treated, and dominant-negative Ezrin–treated cells (fig. S8, L and M). Together, these results suggest that the ERM proteins are a marker of the compartment traversed by NOTCH2 shortly after GSI washout, but they do not themselves substantially modulate NOTCH2 signaling in these cells.

At the 15-min time point after GSI washout, the enrichment of ERM proteins had abated, and there was a period when relatively few proteins showed an enrichment in labeling greater than twofold when compared with baseline labeling in the presence of GSI (Fig. 4C). Although an increase in labeling of motor and cytoskeletal proteins was observed, the effect was small. The lack of strong enrichment of any particular motor protein or complex suggests that NICD2 is primarily cytoplasmic and is not bound to and actively transported by a motor protein through the cytosol to the nuclear membrane after liberation by γ-secretase. In the 5 to 15-min time window, the enrichment of proteins that participate in nuclear import of cargo (Fig. 4D) (*49*, *50*), including the importin β subunit KPNB1 (*51*) and its associated adaptor importin-7, as well as importin α subunits (KPNA1, KPNA2, and KPNA6) and the nuclear pore protein RANBP2 (also called Nup358), suggested that the nuclear import machinery facilitates the NICD2 nuclear entry step. This interpretation is consistent with previous work implicating nuclear import in facilitating the nuclear entry of human Notch1 (*52*) and *Drosophila* Notch (*53*).

NICD2 is nuclear and associated with active transcription within 2 hours after cleavage by γ-secretase

Several proteins exhibited a late labeling pattern with a strong peak enrichment at 2 hours (Fig. 5, A and B). MAML1, a component of Notch transcriptional complexes (*29*, *30*, *54*), was the most significantly enriched protein at this time point when compared with the baseline GSI condition (Fig. 5A), indicative of NICD2 nuclear entry (Fig. 5A). Analysis of the kinetics of MAML1 enrichment showed that increased labeling began at 30 min and was maximal by the 2-hour time point (Fig. 1E).

Most of the other proteins that showed significant, robust enrichment by 2 hours were also implicated in transcriptional regulation or chromatin modification or remodeling (Fig. 5, A and B). Hierarchical clustering revealed that the pattern of enrichment seen for MAML1 was shared by other transcriptional regulators, including RAI1, TCF20, and FUBP1 (Fig. 5B). Likewise, ARID1A and ARID1B, members of the mammalian SWI/SNF chromatin remodeling complex BAF, exhibited the same dynamics of labeling enrichment in this experiment. A similar time course of enrichment was also observed for FUS and EWSR1, both of which are members of the FET (FUS, EWSR1, and TAF15) family of proteins that enter nuclear condensates and can influence transcription, and for several heterogeneous nuclear ribonucleoproteins (HNRNPs) implicated in the regulation of splicing (Fig. 5B) (*55*, *56*). Analysis of quantitative reverse transcription polymerase chain reaction (qRT-PCR) data for the direct Notch target genes *HES1*, *MYC*, and *TRIB1* as a function of time after inhibitor removal showed that Notch-dependent transcriptional induction also occurred as early as 30 min after GSI washout (fig. S9, A to C). Together, these data indicate that NICD2 can initiate the induction of a transcriptional response as early as 30 min after GSI washout and that the response is robust within 2 hours, consistent with other reports showing that dynamic Notch binding sites in the genome become loaded with NICD and other cofactors within 2 hours (*55*–*58*).

To further refine the temporal sequence of association of nuclear factors with NICD2, we acquired a second proximity labeling dataset focusing on time points between 30 min and 4 hours after GSI washout (Fig. 5C and fig. S9, D and E). In this experiment, MAML1, CREBBP/p300, the nuclear factor 1 C-type protein NFIC, and proteins of the BAF chromatin remodeling complex, including ARID1A, ARID1B, SMRCA5, and SMARCC1 (Fig. 5, D to F), showed enrichment by the 45-min time point, reaching maximum enrichment at the 2- and 4-hour time points (see data file S4 for full quantification data of all proteins identified in this dataset). Enrichment of RAI1, HNRNPs, and FET proteins began shortly after the initiation of BAF labeling, at 1 hour (Fig. 5, D to G), indicative of the presence of NICD2 at loci of active transcription by this time point, consistent with the transcriptional induction of Notch-responsive genes observed by qRT-PCR (fig. S9, A to C).

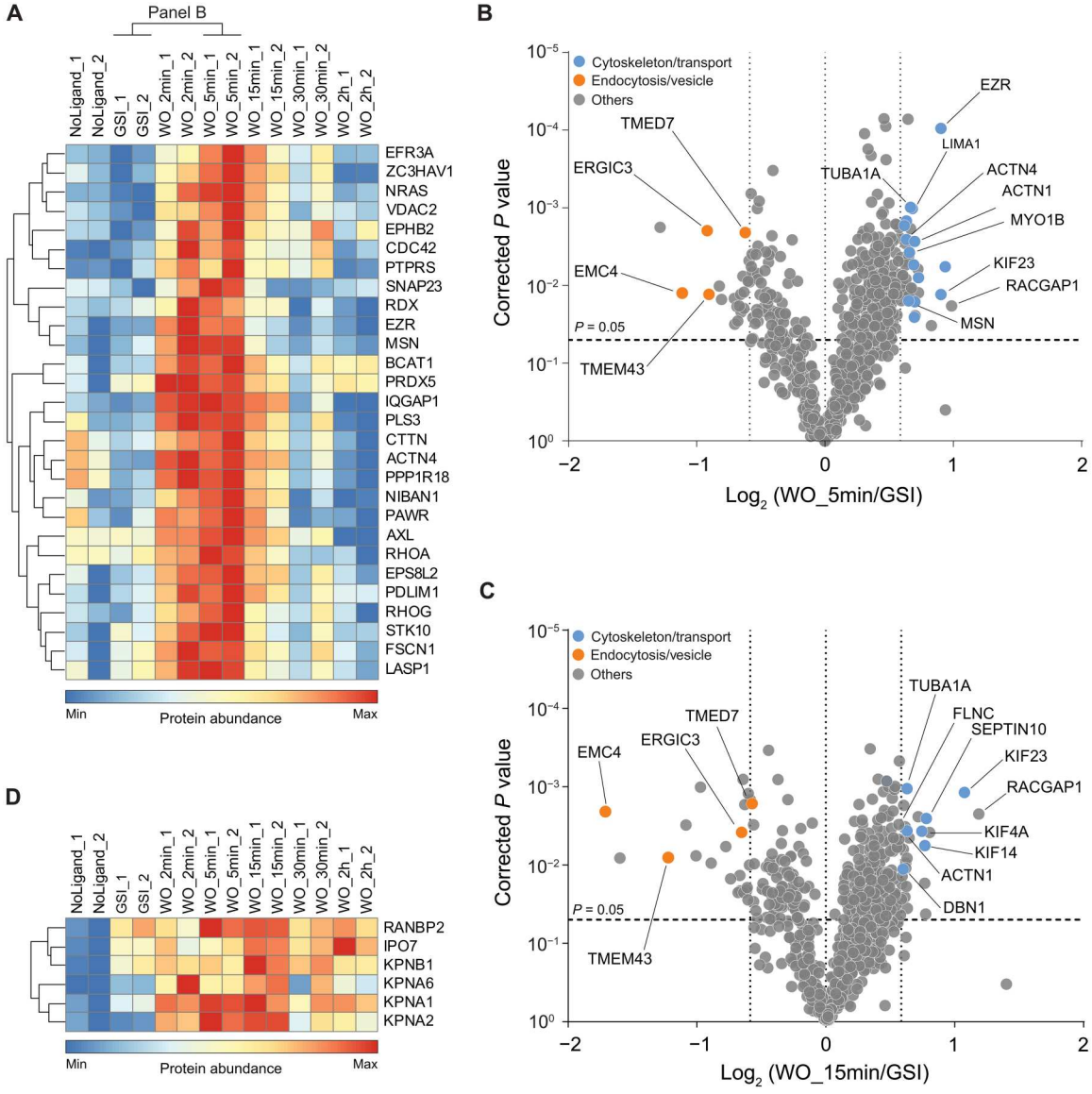

Fig. 4. NICD2 is proximal to ERM proteins early after GSI washout. (**A**) Hierarchical clustering of the proteins characterized by a peak of relative abundance between 2 and 5 min after GSI removal, focusing on neighbors closest to ezrin (EZR). (**B** and **C**) Volcano plots comparing NOTCH2 proximity-labeled proteins enriched at the 5 min (B) and 15 min (C) time points after GSI removal when compared with GSI ($t = 0$). Proteins related to actin, myosin, or cytoskeletal transport are labeled in blue, and proteins related to endocytosis or vesicular-mediated transport are labeled in orange. *P* values are Benjamini-Hochberg–corrected ($P \leq 0.05$, FC ≥ 1.5). (**D**) Heatmap showing the enrichment pattern of proteins related to nuclear import identified by NOTCH2 proximity labeling. Data in all panels are from simultaneous MS analysis of 14 samples from one labeling time course ($n = 1$), with two technical replicates analyzed for each time point.

DISCUSSION

The overarching goal of this work was to achieve high spatiotemporal resolution for the molecular neighborhood of Notch as it transits from membrane to nucleus after proteolytic activation, because there is no real-time dynamic analysis available for this process. Our overall approach was to use NOTCH2-APEX2 time-resolved proximity labeling coupled with quantitative multiplexed proteomics to track the molecular microenvironment of endogenous NOTCH2 as a function of time after ligand stimulation and washout of a GSI. This unbiased approach allowed us to measure dynamic changes in the proteins in proximity to Notch before and after cleavage by γ-secretase, investigate the path and mode of transport of activated NOTCH2 from the membrane to the nucleus, and define the nuclear microenvironment of NICD2 during transcriptional induction.

Because soluble ligands do not activate Notch, it was not possible to use acute addition of the ligand to initiate the signal. It was necessary, therefore, to use GSI washout to achieve the temporal resolution required for dynamic analysis of the Notch molecular neighborhood. Cells were incubated overnight on immobilized ligand in the presence of the GSI because the process of removing cells from a tissue culture dish and transferring them to another dish triggers Notch proteolysis independent of ligand (*59*, *60*). By allowing the cells to incubate overnight on the immobilized ligand

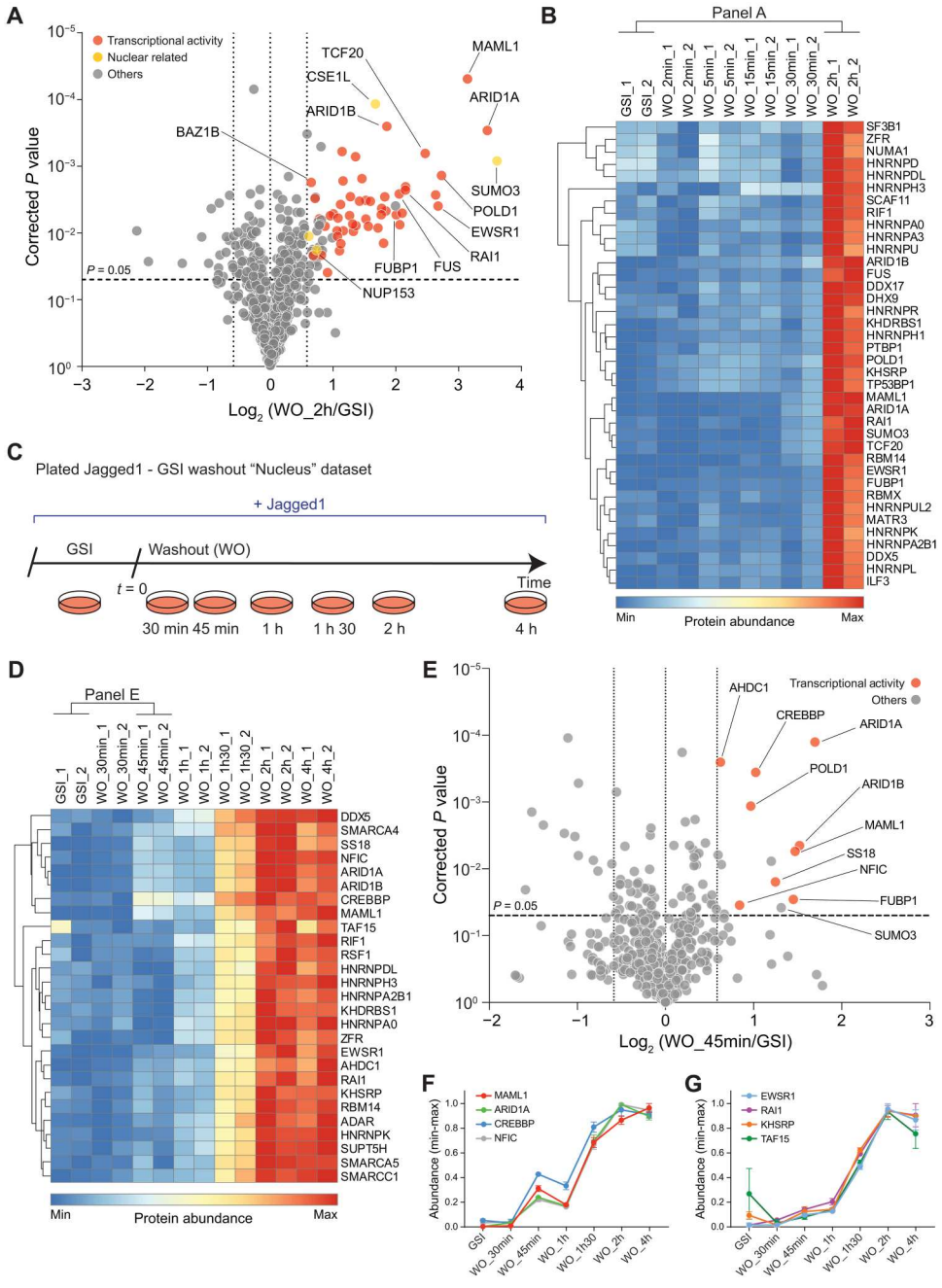

Fig. 5. Nuclear accumulation of NICD2 and engagement with transcriptional regulators. (**A**) Volcano plot highlighting NOTCH2 proximity-labeled proteins enriched 2 hours after GSI removal when compared with GSI ($t = 0$). Significantly enriched proteins ($P \leq 0.05$, FC ≥ 1.5) implicated in transcriptional activity are in red, and other nuclear proteins are indicated in yellow. *P* values are Benjamini-Hochberg–corrected. (**B**) Heatmap showing kinetic profiles of proteins that cluster adjacent to MAML1 with strong enrichment 2 hours after GSI washout. (**C**) Schematic showing the design for focused proximity labeling around the time of NICD2 nuclear entry using immobilized JAG1 as ligand and washout of GSI at time $t = 0$. (**D**) Heatmap of hierarchical clustering centered on proteins with kinetic profiles most closely related to MAML1 in the nuclear-centered proximity labeling dataset (fig. S6). (**E**) Volcano plot of NOTCH2 proximity-labeled proteins enriched 45 min after GSI removal when compared with GSI ($t = 0$) in the nuclear-centered dataset. Significantly enriched proteins ($P \leq 0.05$, FC ≥ 1.5) implicated in transcriptional activity are in red. *P* values are Benjamini-Hochberg–corrected. (**F** and **G**) Line plots showing the kinetic profiles of MAML1, ARID1A, CREBBP/p300, and NFIC (F) and additional transcriptional regulators EWSR1, RAI1, KHSRP, and TAF15 (G) in the nuclear-centered dataset. Data in (A) and (B) are from simultaneous MS analysis of 14 samples from one labeling time course ($n = 1$), with two technical replicates analyzed for each time point. Data in (D) to (G) are from simultaneous MS analysis of 14 samples from a different labeling time course ($n = 1$), with two technical replicates analyzed for each time point.

in the presence of GSI, we made sure that the NOTCH2 protein tracked in the proximity-labeled analysis would be in the NEXT form, with GSI washout synchronizing access to γ-secretase and enabling direct tracking of downstream steps as a function of time. Although we appreciate that accumulating Notch in the NEXT form is a minor limitation of the study, a particular strength of this design is that it enabled time-resolved analysis of proximity with NOTCH2 at natural abundance. The synchronization achieved with GSI removal allowed us to monitor the molecular neighborhood of NOTCH2 as a function of time after inhibitor removal, as judged by the observation that the enrichment of MAML1 in the molecular neighborhood of NOTCH2 only occurred 30 min or more after GSI removal. This timing of nuclear access of NOTCH2 is concordant with that seen in other studies (*11*, *61*).

Several mechanistic findings emerged from these studies. First, the enrichment of proteins associated with vesicular transport and endocytosis after ligand exposure in GSI-treated cells suggested that γ-secretase cleavage of NOTCH2 occurs in an intracellular compartment. This conclusion was supported by additional experiments tracking γ-secretase cleavage activity after washout of inhibitors of ligand-dependent metalloprotease (S2) cleavage in the presence of inhibitors of endocytosis or vesicle acidification, which showed that S2-processed NOTCH2 must enter an intracellular compartment to be cleaved by γ-secretase. Whereas previous studies have reached differing conclusions about whether γ-secretase processes substrates at the plasma membrane (*12*, *13*) or in an intracellular compartment (*14*–*16*), our finding that γ-secretase cleavage of NOTCH2 occurred in an intramembrane compartment agrees with proteomics studies investigating APP cleavage using affinity capture of the early endosome–associated protein EEA, in which the APP cleavage product of γ-secretase (Aβ) accumulates in early/sorting endosomes (*62*).

Second, our data suggest that NOTCH2 molecules transiently pass through a microenvironment enriched in ERM proteins between 2 and 5 min after GSI washout. These proteins appear to identify a compartment traversed by NOTCH2 upon or immediately after γ-secretase cleavage to generate NICD2. In comparison, few proteins are enriched at the 15 and 30 min time points, consistent with the idea that NICD2 moves by passive diffusion to the nucleus after γ-secretase cleavage, with a possible preference for migration in proximity to or along actin filaments, before engaging the nuclear import machinery.

Third, we found that NICD2 entered a nuclear microenvironment enriched in components associated with a transcriptional response as early as 30 to 45 min after GSI washout and that the molecular neighborhood associated with NICD2 persisted

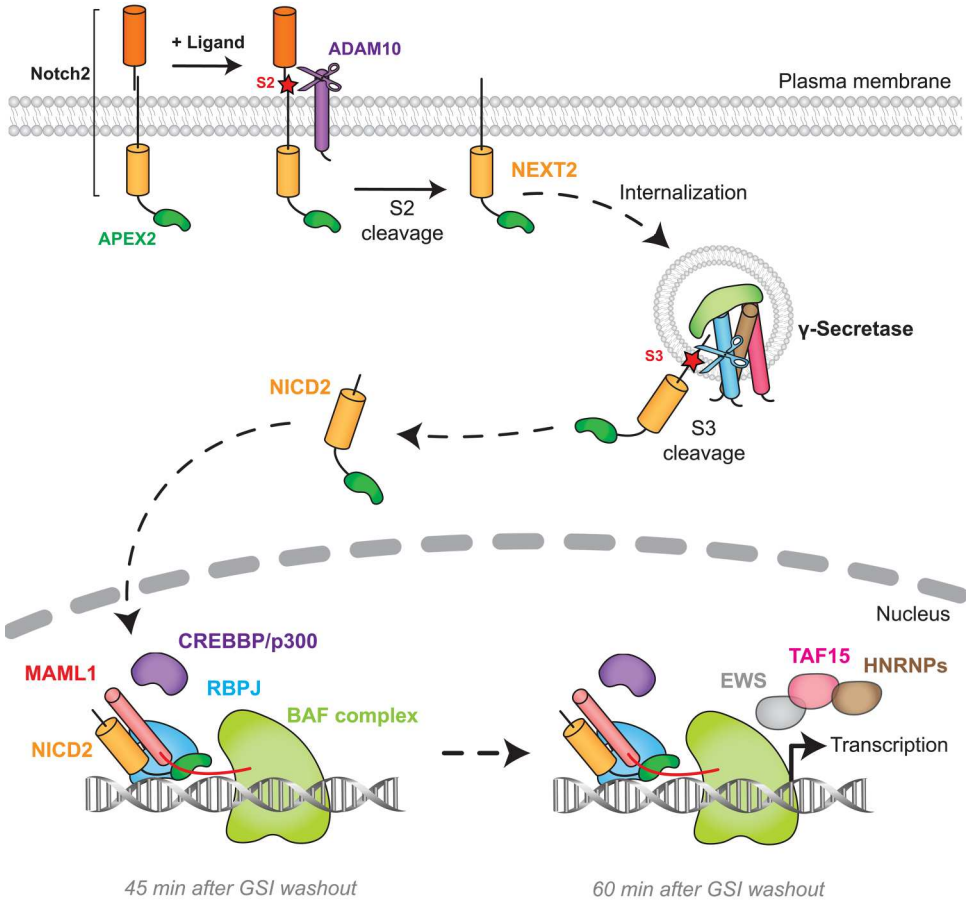

Fig. 6. Model showing NOTCH2 internalization as a mechanistic step in Notch activation and signaling. Upon ligand stimulation of SVG-A cells, NOTCH2 is cleaved at site S2 by ADAM10, followed by entry of S2-processed NOTCH2 (NEXT2) molecules into an intracellular compartment. Internalized NEXT2 molecules are then cleaved at site S3 by γ-secretase, generating NICD2, which accesses the nucleus about 30 to 45 min after GSI washout and induces transcriptional responses.

through the final 4-hour time point. This timing of transcriptional induction is consistent with previous real-time luciferase complementation studies using ectopic NOTCH1 and RBPJ expression (*11*) and with the onset and duration of Notch-induced transcription in fly models and in cancer cells (*59*, *63*–*65*). In addition to MAML1, the nuclear proteins most rapidly recruited to NICD2 were CREBBP/p300, a well-established partner of MAML1 in NICD-dependent transcriptional induction (*57*, *58*, *66*, *67*), and components of the BAF chromatin remodeling complex. The SWI/SNF chromatin remodeling complex is crucial to render enhancers responsive to Notch in *Drosophila* (*56*); the basis for recruitment of the homologous BAF complex to Notch-responsive elements in mammalian cells should be fertile ground for future study.

It is also notable that proteins implicated in NICD degradation were not identified in this study. Because the association of NICD2 with proteins that participate in its degradation may take place transiently and in catalytic amounts, it is possible that our studies were not sensitive enough to identify these interactions.

Overall, our proximity labeling studies and follow-up cellular assays serve as the basis for a well-defined spatiotemporal model of the pathway traversed by Notch upon proteolytic activation (Fig. 6). Ligand engagement first induces S2 cleavage of Notch at the cell surface, followed by entry of truncated NOTCH2 (NEXT2) into an endocytic compartment for cleavage by γ-secretase. As early as 30 min after γ-secretase cleavage, NICD enters the nucleus and by 45 min has begun to recruit CREBBP/p300 and chromatin remodeling complexes to initiate transcription of responsive genes, with evidence for recruitment of proteins involved in transcription-coupled splicing events after 60 to 90 min. More broadly, our work with Notch as a signaling protein of interest represents a proof of concept for future quantitative analyses of other signal transduction systems, showing that time-resolved proximity labeling with APEX2 combined with multiplexed proteomics can elucidate the temporal and spatial dynamics of endogenous proteins and the evolution of their microenvironments during signaling.

MATERIALS AND METHODS

Cell line generation, cultivation, and manipulation

All cell lines were maintained in Dulbecco's modified Eagle's medium (DMEM) with L-glutamine (Corning) supplemented with 10% fetal bovine serum (FBS; Gemini Biosciences) and 1% penicillin-streptomycin (Gibco) at 37°C and 5% CO_2. Cell lines were tested for mycoplasma on a regular basis. CRISPR-Cas9 gene editing was used to knock out NOTCH2 in SVG-A cells. For the SVG-A NOTCH2 knockout cell line, a pX459 plasmid containing a gene-specific guide RNA (gRNA) was transfected using Lipofectamine 2000 (Thermo Fisher Scientific) according to the manufacturer's instructions (see table S2 for gRNA sequences used in this study). Forty-eight hours after transfection, cells were selected using puromycin (2 μg/ml) for 3 days, and single cells were then isolated by flow cytometry using a BD FACSAria cell sorter. Knockout clones were identified by DNA sequencing after PCR amplification of genomic DNA at the mutated locus, and the loss of protein expression was confirmed by Western blotting.

CRISPR-Cas9 genome editing was also used to fuse an APEX2-HA tag at the C terminus of endogenous NOTCH2 in SVG-A cells. SVG-A cells were cotransfected with a pX459 plasmid containing gRNA targeting NOTCH2 (see table S2 for gRNA sequences) and a pUC19 donor plasmid containing a GGAG linker–APEX2–HA–T2A–mNeonGreen cassette flanked by NOTCH2 genomic locus homology arms each approximately 1 kb in length. Seven days after transfection, single cells expressing mNeonGreen were isolated by FACS using a Sony SH800S cell sorter, and individual clones were expanded in 96-well plates. Confirmation of successful tagging and identification of homozygous clones were carried out by PCR amplifying the region of the insertion with flanking primers outside of the genomic region covered by the homology arms, followed by Sanger DNA sequencing for the positive homozygous clones. Clones were further evaluated to assess the amount of expressed NOTCH2 protein by Western blotting, the amount of surface staining by flow cytometry on a BD Accuri C6 Plus flow cytometer, NOTCH2 transcriptional activity using a luciferase reporter assay (described below), and APEX2-dependent protein biotinylation by Western blotting using StrepTactin–horseradish peroxidase (HRP) (Bio-Rad). A similar strategy and gRNA were used to insert a HaloTag at the C terminus of endogenous NOTCH2.

RNA extraction, RT, and qRT-PCR

RNA was harvested from confluent wells of a 12-well plate and isolated using TRIzol (Ambion) according to the manufacturer's instructions. All samples were deoxyribonuclease (DNase)–treated by incubating the extracts with DNase I recombinant (Roche) at 37°C for 30 min. After RNA was recovered from sequential 24:1 chloroform:isoamyl alcohol (Sigma-Aldrich) and ethanol precipitations, RT was performed using an iScript kit (Bio-Rad) according to the manufacturer's instructions with 250 ng of purified RNA as template. qPCR was done in 10 μl of reaction mix with 0.25 μM forward and reverse primers using the PowerUp SYBR Green Master Mix (Thermo Fisher Scientific) with standard thermocycler parameters on a Bio-Rad CFX384 qPCR instrument. A melting curve step right after the PCR amplification was performed to confirm primer specificity. Three technical replicates for each of three biological replicates were analyzed. The primer sequences are listed in table S3. Gene expression was normalized to glyceraldehyde-3-phosphate dehydrogenase (GAPDH) for each condition. For the time-resolved GSI washout experiments presented in fig. S9 (A to C), the data were normalized to the control condition (no ligand conditions in GSI washout), which was assigned a value of 1.

Western blotting

Adherent cells were washed in ice-cold Dulbecco's phosphate-buffered saline (DPBS) and lysed in gel-loading buffer [2% SDS, 60 mM tris-HCl (pH 6.8), 100 mM dithiothreitol (DTT), 10% glycerol, and 0.005% bromophenol blue], scraped off the plate, boiled at 95°C for 5 min, and subjected to SDS–polyacrylamide gel electrophoresis (SDS-PAGE). Proteins were then transferred to a PROTRAN 0.2-μm nitrocellulose membrane (Cytiva) and stained with Ponceau S (Sigma-Aldrich). Membranes were incubated in 5% (w/v) nonfat dry milk in TBST [20 mM tris, 150 mM NaCl, and 0.2% Tween 20 (pH 7.6)] at room temperature for at least 1 hour. Blocked membranes were incubated with various primary antibodies, or with a StrepTactin-HRP (Bio-Rad), diluted in TBST supplemented with 5% nonfat dry milk overnight at 4°C with gentle shaking. Membranes were washed three times with TBST at room temperature and incubated with appropriate secondary antibodies for 1 hour

at room temperature with gentle shaking. Blots were washed three times with TBST and imaged using the Odyssey Infrared Imaging System (LI-COR Biosciences) for IRDye-conjugated secondary antibodies or on a Chemidoc (Bio-Rad) using an Amersham ECL Western Blotting Detection kit (GE Healthcare) for StrepTactin-HRP. See table S1 for a list and working conditions of the antibodies used in this study.

Recombinant JAG1-Fc expression and purification

The extracellular domain (ECD) of human JAG1 (amino acids 1 to 1067) was fused to the Fc region (CH2 and CH3 domains) and hinge region of the human immunoglobulin G1 (IgG1) heavy chain in the pFUSE-Fc1 vector (InvivoGen). JAG1ECD-Fc protein was expressed in Expi293F cells grown in Expi293F expression medium at 37°C in an 8% CO_2 incubator with constant shaking. Cells were grown to a density of 3×10^6 cells/ml in a final volume of 1 liter and transiently transfected using FectoPro transfection reagent (Poly-plus) with 1 mg of purified plasmid at a 2:1 DNA/FectoPro ratio. Twenty-two hours after transfection, 5 mM valproic acid sodium salt (Sigma-Aldrich) and 10 ml of 45% D-(+)-glucose solution (Sigma-Aldrich) were added. After 7 days of culture, the medium supernatant was collected after removal of debris by centrifugation at 4000*g* for 15 min at 4°C followed by a filtration step. Filtered medium was then loaded onto a Protein A (Millipore) column prewashed in ice-cold Hepes-buffered saline (HBS) buffer [20 mM Hepes (pH 7.3) and 150 mM NaCl]. Bound protein was eluted in 100 mM glycine (pH 3.0) and neutralized with 1 M tris buffer (pH 7.3). Eluted protein was buffer-exchanged and concentrated in HBS. Protein purity was assessed by separation on SDS-PAGE after staining with SafeBlue (Thermo Fisher Scientific). The purified protein was diluted to a final concentration of 200 μg/ml in HBS supplemented with 10% glycerol, aliquoted, flash-frozen, and stored at −80°C.

Activation of NOTCH2 by immobilized JAG1-Fc

Recombinant JAG1-Fc was immobilized by overnight incubation at 4°C in individual wells of non–tissue culture–treated 6- or 12-well plates (VWR) at a final concentration of 2 μg/ml in DPBS containing poly-D-lysine (10 μg/ml; Thermo Fisher Scientific). For imaging studies, the ligand was immobilized in 24-well plates containing prewashed glass coverslips overnight. The next day, the JAG1-Fc and poly-D-lysine mixture was removed, and the cells were added to the coverslips and incubated as indicated.

Luciferase reporter assays

SVG-A cells were transfected with a mixture of TP1–firefly luciferase and pRL-TK (Promega) plasmids at a 49:1 ratio using Lipofectamine 2000 (Thermo Fisher Scientific) according to the manufacturer's instructions. The culture medium was replaced 4 hours after transfection, and the cells were incubated overnight. The next day, cells were detached with 0.5 mM EDTA, recovered by centrifugation, and added to plates precoated with recombinant JAG1-Fc in medium containing 100 nM Compound E (GSI) or 5 μM GI25X. At that time, luciferase assays were performed using a dual-luciferase reporter assay system (Promega) according to the manufacturer's instructions. For experiments investigating the effects of endocytosis or vesicular acidification, cells were preincubated with hydroxy-dynasore, BafA1, or chloroquine for 1 hour before removal of GI25X, and cells were harvested 6 hours later. Luminescence was measured on a GloMax plate reader (Promega). Three technical measurements were performed for each of three biological replicates. The ratio of firefly to *Renilla* luminescence was calculated normalized to the control condition (presence of GI25X and dimethyl sulfoxide) and assigned a value of 100%.

Flow cytometry

Cells were washed with DPBS, detached using 0.5 mM EDTA in DPBS for 5 min at room temperature, pelleted, and washed again with DPBS. For permeabilized conditions, cells were fixed in 0.01% formaldehyde in DPBS for 15 min at room temperature, washed, then incubated in 0.5% (v/v) Tween 20 in DPBS for 5 min at room temperature, and finally washed once again. Cells were then incubated for 45 min at 4°C in the dark with 2 μl of the appropriate antibody diluted in 2% (v/v) FBS in DPBS. Cells were then washed twice with DPBS and analyzed on a BD Accuri C6 Plus flow cytometer.

APEX2 proximity labeling

SVG-A NOTCH2-APEX2-HA cells were incubated overnight on tissue culture dishes in the presence of immobilized JAG1 or with JAG1-expressing A673 cells in the presence of 100 nM GSI or 10 μM BB94. The next day, cells were washed three times with DMEM to remove the inhibitor. The time of addition of fresh medium after the last wash was set to $t = 0$ in defining the time points analyzed in each experiment. For each time point, the medium was exchanged with fresh medium containing an additional 2 mM biotin phenol (Iris Biotech GmbH, LS-3500) exactly 1 hour before 0.1 mM hydrogen peroxide (H_2O_2; Sigma-Aldrich) was added to initiate the labeling reaction. Immediately after adding H_2O_2, the culture dishes were gently rocked several times to ensure optimal H_2O_2 distribution. Exactly 1 min after the addition of H_2O_2, the medium was quickly aspirated, and cells were washed three times with quenching buffer [DPBS supplemented with 10 mM sodium ascorbate, 5 mM Trolox (Sigma-Aldrich), and 10 mM sodium azide]. Cells were then scraped in quenching buffer and harvested by centrifugation, and cell pellets were flash-frozen and stored at −80°C until streptavidin pull-down was performed. An H_2O_2 stock solution (30%, v/v) was freshly diluted to 1 M in DPBS immediately before each experiment. See table S1 for a list of key reagents used for the proximity labeling.

Streptavidin pull-down

All solutions and buffers were freshly prepared and filtered. Streptavidin capture of biotinylated proteins was performed as previously described (*22*, *68*). Briefly, frozen cell pellets were lysed in ice-cold lysis buffer [8 M urea, 100 mM sodium phosphate (pH 8.0), 1% SDS (w/v), 100 mM NH_4HCO_3, 10 mM tris(2 carboxyethyl)phosphine (TCEP)] and pipetted repeatedly on ice to ensure proper cell lysis. Lysates were then homogenized by passing them through QIAshredder cartridges (Qiagen). Proteins were precipitated by adding an equal volume of ice-cold 55% trichloroacetic acid (Sigma-Aldrich), incubated for 15 min on ice, and then pelleted by centrifugation at 21,000*g* at 4°C for 10 min. The protein pellet was washed with −20°C cold acetone (Sigma-Aldrich), vortexed, and centrifuged at 21,000*g* at 4°C for 10 min. After centrifugation, acetone was removed, and the pellet was washed with acetone three more times. After the last wash, the pellet was resuspended in lysis buffer as described above, vortexed, and rotated at room

temperature until fully dissolved, allowing reduction of proteins by TCEP at the same time.

Resuspended proteins were centrifuged at 21,000*g* at room temperature for 10 min, and the clear supernatant was transferred to a new microcentrifuge tube. To alkylate free cysteines, freshly prepared 400 mM iodoacetamide stock solution (Sigma-Aldrich) in 50 mM ammonium bicarbonate was added to the supernatant at a final concentration of 20 mM, and the samples were immediately vortexed and then incubated in the dark at room temperature for 25 min. After alkylation, freshly prepared DTT (Sigma-Aldrich) was added to a final concentration of 50 mM to quench the reaction. Last, water was added to each sample to reach a final concentration of 4 M urea and 0.5% (w/v) of SDS.

Streptavidin magnetic bead suspension (125 μl) (Thermo Fisher Scientific) was washed twice with 4 M urea, 0.5% SDS (w/v), and 100 mM sodium phosphate (pH 8.0) and added to each sample. The tubes were gently rotated overnight at 4°C. After capture of biotinylated proteins, the magnetic beads were washed three times with 4 M urea, 0.5% SDS (w/v), and 100 mM sodium phosphate (pH 8.0); three more times with the same buffer without SDS; and finally three more times with DPBS. The beads were transferred to new tubes for each change of wash buffer. See table S1 for a list of key reagents used for the streptavidin enrichment of biotinylated proteins.

On-bead digestion and TMT labeling

The streptavidin beads were subjected to on-bead protease digestion in 50 μl of digestion buffer [200 mM EPPS (pH 8.5) with 2% acetonitrile (v/v)] along with LysC (Wako) at an enzyme-to-substrate ratio of 1:50. The samples were incubated at 37°C for 3 hours. Then, 50 μl of digestion buffer with trypsin (Promega) was added at an enzyme-to-substrate ratio of 1:100. The digestion was continued at 37°C overnight with gentle agitation. The clear supernatants of digested protein were separated from beads with a magnetic rack and transferred to fresh tubes.

For the tandem mass tag (TMT) reaction, 30% acetonitrile (v/v) was added to the digested protein and then labeled using a TMT isobaric mass tagging kit (Thermo Fisher Scientific). The TMT reaction was performed for 1 hour according to the manufacturer's instructions. TMT labeling efficiency and ratios were measured by liquid chromatography–MS3 (LC-MS3) analysis after combining equal volumes from each sample. Once the labeling efficiency was determined to be >95%, the TMT reactions were quenched with hydroxylamine 0.5% (v/v) for 15 min and acidified with formic acid. Samples were then pooled and dried to near completion under reduced pressure before resuspension in 1% formic acid and fractionation using the Pierce High pH Reversed-Phase Peptide Fractionation Kit (Thermo Fisher Scientific) with modified elution of 12 sequential fractions (10, 12.5, 15, 17.5, 20, 25, 30, 35, 40, 50, 65, and 80% acetonitrile). Fractions were then combined into pairs as follows, 1 + 7, 2 + 8, 3 + 9, 4 + 10, 5 + 11, and 6 + 12, to give the final six fractionated samples. The resulting fractions were dried under reduced pressure and then desalted using a stage tip protocol (*69*).

MS acquisition and data analysis

Data were acquired on an Orbitrap Fusion Lumos instrument (Thermo Fisher Scientific) coupled to a Proxeon Easy-nLC 1200 ultrahigh-performance LC. Peptides were injected onto a 100-μm (inner diameter) capillary column (~30 cm) packed in-house with C18 resin (2.6 μm, 150 Å, Thermo Fisher Scientific). Peptide fractions were separated with a 4-hour acidic acetonitrile gradient from 5 to 35% buffer B (buffer A = 0.125% formic acid, buffer B = 95% acetonitrile, 0.125% formic acid). All data were collected with a multinotch MS3 method (*70*). MS1 scans (Orbitrap analysis; resolution, 120,000; mass range, 400 to 1400 Th) were followed by MS2 analysis with collision-induced dissociation [collision energy (CE) = 35] and a maximum ion injection time of up to 120 ms and an isolation window of 0.4 mass/charge ratio (m/z), using rapid scan mode. To obtain quantitative information, MS3 precursors were fragmented by high-energy collision-induced dissociation (CE = 65) and analyzed in the Orbitrap at a resolution of 50,000 at 200 Th with maximum injection time set to 650 ms. Raw spectra were converted to mzXML to correct monoisotopic m/z measurements and to perform a postsearch calibration.

Spectra were searched using SEQUEST (v.28, rev.12) software against the UniProt human reference proteome (downloaded on 25 February 2020), containing common contaminants and reversed order protein sequences as decoy hits (*71*). Searches were performed with a precursor mass tolerance of 20 parts per million, and the fragment-ion tolerance was set to 0.9 Da. For searches, a maximum of two missed trypsin cleavage sites were allowed. Methionine oxidation (+15.9949 Da) was set as a variable modification, whereas cysteine carboxyamidomethylation (+57.0215) and TMT (+229.1629) or TMT16 (+304.2071 Da) tags on lysine and peptide N-termini were set as a static modification. Peptide spectral matches (PSMs) were filtered by linear discriminant analysis (LDA), using a target-decoy database search to adjust the PSM false discovery rate (FDR) to 1% and protein level FDR of 1% (*72*). For MS3 relative quantification, peptides were filtered for an MS2 isolation specificity of >70%, and a total TMT summed signal to noise of >200 for all channels in the multiplex. Further details of the TMT quantification method and search parameters applied were described previously (*73*). Proteomics raw data and search results were deposited in the PRIDE archive for each multiplex experiment with the following accession numbers: PXD039008 (immobilized ligand with GSI experiment; data file S1), PXD042123 (coculture with JAG1-expressing A673 cells; data files S2 and S3), and PXD039010 (immobilized ligand with GSI nuclear-centered experiment; data file S4).

Hydroxy-dynasore, BafA1, and chloroquine treatments

For immunofluorescence experiments, Western blots, and reporter gene assays using hydroxy-dynasore (Sigma-Aldrich), BafA1 (Selleck Chemicals), or chloroquine (Sigma-Aldrich), cells were incubated overnight on immobilized JAG1 in the presence of GSI or GI25X. The next day, hydroxy-dynasore (Sigma-Aldrich), BafA1, or chloroquine was added to the medium and preincubated with the culture for 1 hour before removing GSI or GI25X. Cells were maintained in the continued presence of hydroxy-dynasore, BafA1, or chloroquine at 37°C for the indicated time before analysis. Hydroxy-dynasore incubation was performed in serum-free DMEM.

Immunofluorescence and image processing

SVG-A NOTCH2-HaloTag cells were grown on ligand-coated coverslips. Cells were labeled with JaneliaFluorX549 HaloTag ligand (a gift from L. Lavis, Janelia Research Campus) at a final concentration of 100 nM in medium for 15 min at 37°C. The medium was then

removed, and cells were washed with fresh medium and returned to the incubator for 1 hour to allow newly synthesized labeled NOTCH2 to be delivered to the plasma membrane. Cells were treated with the indicated vesicular/transport inhibitors before GI25X/GSI washout, as described above, before imaging.

For immunofluorescence studies, cells were washed three times in DPBS 2 hours after washout of GI25X or GSI, fixed with 4% paraformaldehyde (Sigma-Aldrich) for 15 min at room temperature, washed three times in DPBS, and quenched with 0.1 M glycine (pH 7.5) in DPBS for 15 min at room temperature. After another three PBS washes, fixed cells were permeabilized with 0.1% Triton X-100 in DPBS for 10 min at room temperature followed by three washes in DPBS and blocking in 5% bovine serum albumin (w/v) in DPBS for 1 hour at room temperature. Cells were then stained for 1 hour at room temperature with an anti-NICD2 primary antibody diluted in blocking buffer (see table S1 for the list of antibodies used in this study). After three washes in DPBS, the cells were incubated with secondary antibody (Alexa Fluor Plus 647–conjugated anti-rabbit, Thermo Fisher Scientific, A32795) diluted in blocking buffer for 45 min at room temperature followed by three washes in DPBS. For DNA staining, cells were incubated with SYTOX Green Nucleic Acid Stain (Thermo Fisher Scientific) according to manufacturer's recommendations followed by three washes in DPBS. Coverslips were then mounted with ProLong Gold Antifade Mountant with 4′,6-diamidino-2-phenylindole (DAPI; Thermo Fisher Scientific) or without DAPI if already labeled with SYTOX Green. Coverslips were stored at 4°C before image acquisition.

Images were acquired using a Marianas system (Intelligent Imaging Innovation) composed of a Zeiss Axio Observer Z1 (Carl Zeiss) equipped with a 63× objective (Plan-Apochromat, numerical aperture 1.4, Carl Zeiss), a spinning disk confocal head (CSU-XI, Yokogawa Electric Corporation), and a spherical aberration correction system (Infinity Photo-Optical). Excitation light was provided by 405-, 488-, 561-, or 640-nm solid-state lasers (Sapphire, 50 mW, Coherent Inc.) coupled to an acoustic-optical tunable filter. Laser power and exposure times were kept the same for all experiments. *Z* stacks of 38 *x*-*y* confocal images were obtained in 270-nm *z*-steps using a cooled QuantEM 512SC charge-coupled device (CCD) camera (Photometrics). Images presented in fig. S6 (effect of ERM proteins on NOTCH2 signaling) were acquired using a Prime 95B Scientific complementary metal oxide semiconductor (CMOS) camera (Photometrics), giving different signal arbitrary units from the ones recorded with the QuantEM 512SC CCD camera used in the other experiments. All equipment was controlled by SlideBook acquisition software (Intelligent Imaging Innovations). Image processing was performed using Fiji software (*74*). For nuclear intensity measurements, the nuclei were identified by DAPI staining, and the mean fluorescence intensity (MFI) of each indicated channel was measured by applying a nucleus mask using Fiji software (*73*).

siRNA-mediated knockdown of ERM proteins and evaluation of dominant-negative ezrin

Silencer Select siRNAs for ezrin (s14795), radixin (s11899), moesin (s8984), and siCtrl AM4611 were all purchased from Thermo Fisher Scientific. For siRNA-mediated knockdown of ERM proteins, the cells were reverse-transfected with the indicated siRNAs using Lipofectamine RNAiMAX transfection reagent according to the manufacturer's recommendations. Parental or NOTCH2-HaloTag SVG-A cells were seeded in a six-well plate along with the transfection mix containing 3 μl of Lipofectamine RNAiMAX and a total of 30 pmol of siRNA in 500 μl of Opti-MEM. A portion of each sample (siCtrl or siERM) from each experiment (immunofluorescence, NICD2 Western blotting, and luciferase reporter assay) was set aside, lysed in gel-loading buffer as already described, and subjected to Western blotting against ezrin, radixin, and moesin to evaluate depletion efficiency. Immunofluorescence analyses and Western blots were performed at 0 (GSI) or 2 hours (WO_2h) after GSI washout as described above. For luciferase reporter experiments, the cells were transfected the next day with a mixture of TP1–firefly luciferase and pRL-TK (Promega) plasmids at a 49:1 ratio using Lipofectamine 2000 (Thermo Fisher Scientific) and read out as described above 24 hours later.

For ezrin dominant-negative experiments, the full-length human ezrin sequence, or a sequence comprising the amino acids 1 to 300, was inserted N-terminal to mNeonGreen in pcDNA3.1. SVG-A NOTCH2-HaloTag cells were transfected in six-well plate format with 2 μg of DNA per well using Lipofectamine 2000 (Thermo Fisher Scientific) according to the manufacturer's instructions. Culture medium was replaced 4 hours after transfection. The next day, the transfected cells were detached and plated on ligand-coated coverslips in the presence of 100 nM GSI and incubated overnight. The following day, the GSI was removed, and the cells were fixed and processed for immunofluorescence as described above.

Statistical analysis

Statistical analyses of fluorescence microscopy, luciferase reporter assays, qRT-PCR, Western blotting, and flow cytometry experiments were performed using GraphPad Prism software (GraphPad). Two-way analysis of variance (ANOVA) followed by Tukey's pairwise comparison was used for statistical comparisons. All error bars denote mean ± SD. $^{*}P \leq 0.05$, $^{**}P \leq 0.01$, and $^{***}P \leq 0.001$. The number of individual experiments analyzed is indicated in the figure legends.

Supplementary Materials

This PDF file includes:
Figs. S1 to S9
Tables S1 to S3

Other Supplementary Material for this manuscript includes the following:
Data files S1 to S4
MDAR Reproducibility Checklist

REFERENCES AND NOTES

1. C. Siebel, U. Lendahl, Notch signaling in development, tissue homeostasis, and disease. *Physiol. Rev.* **97**, 1235–1294 (2017).
2. K. Hori, A. Sen, S. Artavanis-Tsakonas, Notch signaling at a glance. *J. Cell Sci.* **126**, 2135–2140 (2013).
3. B. M. Kamath, R. C. Bauer, K. M. Loomes, G. Chao, J. Gerfen, A. Hutchinson, W. Hardikar, G. Hirschfield, P. Jara, I. D. Krantz, P. Lapunzina, L. Leonard, S. Ling, V. L. Ng, P. le Hoang, D. A. Piccoli, N. B. Spinner, NOTCH2 mutations in Alagille syndrome. *J. Med. Genet.* **49**, 138–144 (2012).
4. L. Li, I. D. Krantz, Y. Deng, A. Genin, A. B. Banta, C. C. Collins, M. Qi, B. J. Trask, W. L. Kuo, J. Cochran, T. Costa, M. E. M. Pierpont, E. B. Rand, D. A. Piccoli, L. Hood, N. B. Spinner, Alagille syndrome is caused by mutations in human Jagged1, which encodes a ligand for Notch1. *Nat. Genet.* **16**, 243–251 (1997).

5. P. D. Turnpenny, N. Whittock, J. Duncan, S. Dunwoodie, K. Kusumi, S. Ellard, Novel mutations in DLL3, a somitogenesis gene encoding a ligand for the Notch signalling pathway, cause a consistent pattern of abnormal vertebral segmentation in spondylocostal dysostosis. *J. Med. Genet.* **40**, 333–339 (2003).
6. M. A. Simpson, M. D. Irving, E. Asilmaz, M. J. Gray, D. Dafou, F. V. Elmslie, S. Mansour, S. E. Holder, C. E. Brain, B. K. Burton, K. H. Kim, R. M. Pauli, S. Aftimos, H. Stewart, C. A. Kim, M. Holder-Espinasse, S. P. Robertson, W. M. Drake, R. C. Trembath, Mutations in NOTCH2 cause Hajdu-Cheney syndrome, a disorder of severe and progressive bone loss. *Nat. Genet.* **43**, 303–305 (2011).
7. J. C. Aster, W. S. Pear, S. C. Blacklow, The varied roles of notch in cancer. *Annu. Rev. Pathol. Mech. Dis.* **12**, 245–275 (2016).
8. N. J. Wang, Z. Sanborn, K. L. Arnett, L. J. Bayston, W. Liao, C. M. Proby, I. M. Leigh, E. A. Collisson, P. B. Gordon, L. Jakkula, S. Pennypacker, Y. Zou, M. Sharma, J. P. North, S. S. Vemula, T. M. Mauro, I. M. Neuhaus, P. E. LeBoit, J. S. Hur, K. Park, N. Huh, P. Y. Kwok, S. T. Arron, P. P. Massion, A. E. Bale, D. Haussler, J. E. Cleaver, J. W. Gray, P. T. Spellman, A. P. South, J. C. Aster, S. C. Blacklow, R. J. Cho, Loss-of-function mutations in Notch receptors in cutaneous and lung squamous cell carcinoma. *Proc. Natl. Acad. Sci. U.S.A.* **108**, 17761–17766 (2011).
9. D. Henrique, F. Schweisguth, Mechanisms of notch signaling: A simple logic deployed in time and space. *Development* **146**, dev172148 (2019).
10. D. Sprinzak, S. C. Blacklow, Biophysics of notch signaling. *Annu. Rev. Biophys.* **50**, 157–189 (2021).
11. M. X. G. Ilagan, S. Lim, M. Fulbright, D. Piwnica-Worms, R. Kopan, Real-time imaging of Notch activation with a luciferase complementation-based reporter. *Sci. Signal.* **4**, rs7 (2011).
12. J. H. Chyung, D. M. Raper, D. J. Selkoe, γ-Secretase exists on the plasma membrane as an intact complex that accepts substrates and effects intramembrane cleavage. *J. Biol. Chem.* **280**, 4383–4392 (2005).
13. E. M. Hansson, K. Strömberg, S. Bergstedt, G. Yu, J. Näslund, J. Lundkvist, U. Lendahl, Aph-1 interacts at the cell surface with proteins in the active γ-secretase complex and membrane-tethered Notch. *J. Neurochem.* **92**, 1010–1020 (2005).
14. N. Gupta-Rossi, E. Six, O. LeBail, F. Logeat, P. Chastagner, A. Olry, A. Israël, C. Brou, Monoubiquitination and endocytosis direct γ-secretase cleavage of activated Notch receptor. *J. Cell Biol.* **166**, 73–83 (2004).
15. G. Chapman, J. A. Major, K. Iyer, A. C. James, S. E. Pursglove, J. L. M. Moreau, S. L. Dunwoodie, Notch1 endocytosis is induced by ligand and is required for signal transduction. *Biochim. Biophys. Acta Mol. Cell Res.* **1863**, 166–177 (2016).
16. F. Kobia, S. Duchi, G. Deflorian, T. Vaccari, Pharmacologic inhibition of vacuolar H^+ ATPase reduces physiologic and oncogenic Notch signaling. *Mol. Oncol.* **8**, 207–220 (2014).
17. H. W. Rhee, P. Zou, N. D. Udeshi, J. D. Martell, V. K. Mootha, S. A. Carr, A. Y. Ting, Proteomic mapping of mitochondria in living cells via spatially restricted enzymatic tagging. *Science* **339**, 1328–1331 (2013).
18. V. Hung, N. D. Udeshi, S. S. Lam, K. H. Loh, K. J. Cox, K. Pedram, S. A. Carr, A. Y. Ting, Spatially resolved proteomic mapping in living cells with the engineered peroxidase APEX2. *Nat. Protoc.* **11**, 456–475 (2016).
19. S. S. Lam, J. D. Martell, K. J. Kamer, T. J. Deerinck, M. H. Ellisman, V. K. Mootha, A. Y. Ting, Directed evolution of APEX2 for electron microscopy and proximity labeling. *Nat. Methods* **12**, 51–54 (2014).
20. J. Paek, M. Kalocsay, D. P. Staus, L. Wingler, R. Pascolutti, J. A. Paulo, S. P. Gygi, A. C. Kruse, Multidimensional tracking of GPCR signaling via peroxidase-catalyzed proximity labeling. *Cell* **169**, 338–349.e11 (2017).
21. A. P. Martin, M. Jacquemyn, J. Lipecka, C. Chhuon, V. N. Aushev, B. Meunier, M. K. Singh, N. Carpi, M. Piel, P. Codogno, A. Hergovich, M. C. Parrini, G. Zalcman, I. C. Guerrera, D. Daelemans, J. H. Camonis, STK38 kinase acts as XPO1 gatekeeper regulating the nuclear export of autophagy proteins and other cargoes. *EMBO Rep.* **20**, e48150 (2019).
22. E. A. May, M. Kalocsay, I. G. D'auriac, P. S. Schuster, S. P. Gygi, M. V. Nachury, D. U. Mick, Time-resolved proteomics profiling of the ciliary hedgehog response. *J. Cell Biol.* **220**, e202007207 (2021).
23. W. Bailis, Y. Yashiro-Ohtani, W. S. Pear, Identifying direct Notch transcriptional targets using the GSI-washout assay. *Methods Mol. Biol.* **1187**, 247–254 (2014).
24. F. A. Ran, P. D. Hsu, J. Wright, V. Agarwala, D. A. Scott, F. Zhang, Genome engineering using the CRISPR-Cas9 system. *Nat. Protoc.* **8**, 2281–2308 (2013).
25. A. Ludwig, C. Hundhausen, M. Lambert, N. Broadway, R. Andrews, D. Bickett, M. Leesnitzer, J. Becherer, Metalloproteinase inhibitors for the disintegrin-like metalloproteinases ADAM10 and ADAM17 that differentially block constitutive and phorbol ester-inducible shedding of cell surface molecules. *Comb. Chem. High Throughput Screen.* **8**, 161–171 (2005).
26. W. R. Gordon, B. Zimmerman, L. He, L. J. Miles, J. Huang, K. Tiyanont, D. G. McArthur, J. C. Aster, N. Perrimon, J. J. Loparo, S. C. Blacklow, Mechanical allostery: Evidence for a force requirement in the proteolytic activation of Notch. *Dev. Cell* **33**, 729–736 (2015).
27. C. Delaney, B. Varnum-Finney, K. Aoyama, C. Brashem-Stein, I. D. Bernstein, Dose-dependent effects of the Notch ligand Delta1 on ex vivo differentiation and in vivo marrow repopulating ability of cord blood cells. *Blood* **106**, 2693–2699 (2005).
28. B. Varnum-Finney, C. Brashem-Stein, I. D. Bernstein, Combined effects of Notch signaling and cytokines induce a multiple log increase in precursors with lymphoid and myeloid reconstituting ability. *Blood* **101**, 1784–1789 (2003).
29. L. Wu, J. C. Aster, S. C. Blacklow, R. Lake, S. Artavanis-Tsakonas, J. D. Griffin, MAML1, a human homologue of *Drosophila* mastermind, is a transcriptional co-activator for NOTCH receptors. *Nat. Genet.* **26**, 484–489 (2000).
30. A. G. Petcherski, J. Kimble, Mastermind is a putative activator for Notch. *Curr. Biol.* **10**, R471–R473 (2000).
31. R. Aber, W. Chan, S. Mugisha, L. A. Jerome-Majewska, Transmembrane emp24 domain proteins in development and disease. *Genet. Res.* **101**, e14 (2019).
32. M. N. J. Seaman, The retromer complex-endosomal protein recycling and beyond. *J. Cell Sci.* **125**, 4693–4702 (2012).
33. V. W. Chow, M. P. Mattson, P. C. Wong, M. Gleichmann, An overview of APP processing enzymes and products. *Neuromolecular Med.* **12**, 1–12 (2010).
34. A. Mccluskey, J. A. Daniel, G. Hadzic, N. Chau, E. L. Clayton, A. Mariana, A. Whiting, N. N. Gorgani, J. Lloyd, A. Quan, L. Moshkanbaryans, S. Krishnan, S. Perera, M. Chircop, L. von Kleist, A. B. Mcgeachie, M. T. Howes, R. G. Parton, M. Campbell, J. A. Sakoff, X. Wang, J. Y. Sun, M. J. Robertson, F. M. Deane, T. H. Nguyen, F. A. Meunier, M. A. Cousin, P. J. Robinson, Building a better dynasore: The dyngo compounds potently inhibit dynamin and endocytosis. *Traffic* **14**, 1272–1289 (2013).
35. T. Kirchhausen, E. Macia, H. E. Pelish, Use of dynasore, the small molecule inhibitor of dynamin, in the regulation of endocytosis. *Methods Enzymol.* **438**, 77–93 (2008).
36. E. Macia, M. Ehrlich, R. Massol, E. Boucrot, C. Brunner, T. Kirchhausen, Dynasore, a cell-permeable inhibitor of dynamin. *Dev. Cell* **10**, 839–850 (2006).
37. T. Yoshimori, A. Yamamoto, Y. Moriyama, M. Futai, Y. Tashiro, Bafilomycin A1, a specific inhibitor of vacuolar-type H^+-ATPase, inhibits acidification and protein degradation in lysosomes of cultured cells. *J. Biol. Chem.* **266**, 17707–17712 (1991).
38. J. Xu, H. T. Feng, C. Wang, K. H. M. Yip, N. Pavlos, J. M. Papadimitriou, D. Wood, M. H. Zheng, Effects of bafilomycin A1: An inhibitor of vacuolar H^+-ATPases on endocytosis and apoptosis in RAW cells and RAW cell-derived osteoclasts. *J. Cell. Biochem.* **88**, 1256–1264 (2003).
39. T. Vaccari, S. Duchi, K. Cortese, C. Tacchetti, D. Bilder, The vacuolar ATPase is required for physiological as well as pathological activation of the Notch receptor. *Development* **137**, 1825–1832 (2010).
40. M. Mauthe, I. Orhon, C. Rocchi, X. Zhou, M. Luhr, K. J. Hijlkema, R. P. Coppes, N. Engedal, M. Mari, F. Reggiori, Chloroquine inhibits autophagic flux by decreasing autophagosome-lysosome fusion. *Autophagy* **14**, 1435–1455 (2018).
41. V. Shanmugam, J. W. Craig, L. K. Hilton, M. H. Nguyen, C. K. Rushton, K. Fahimdanesh, S. Lovitch, B. Ferland, D. W. Scott, J. C. Aster, Notch activation is pervasive in SMZL and uncommon in DLBCL: Implications for Notch signaling in B-cell tumors. *Blood Adv.* **5**, 71–83 (2021).
42. J. C. Aster, L. Xu, F. G. Karnell, V. Patriub, J. C. Pui, W. S. Pear, Essential roles for ankyrin repeat and transactivation domains in induction of T-cell leukemia by Notch1. *Mol. Cell. Biol.* **20**, 7505–7515 (2000).
43. J. M. Rogers, B. Guo, E. D. Egan, J. C. Aster, K. Adelman, S. C. Blacklow, MAML1-dependent notch-responsive genes exhibit differing cofactor requirements for transcriptional activation. *Mol. Cell. Biol.* **40**, e00014-20 (2020).
44. R. G. Fehon, A. I. McClatchey, A. Bretscher, Organizing the cell cortex: The role of ERM proteins. *Nat. Rev. Mol. Cell Biol.* **11**, 276–287 (2010).
45. S. Louvet-Vallée, ERM proteins: From cellular architecture to cell signaling. *Biol. Cell* **92**, 305–316 (2000).
46. D. Chirivino, L. del Maestro, E. Formstecher, P. Hupé, G. Raposo, D. Louvard, M. Arpin, The ERM proteins interact with the HOPS complex to regulate the maturation of endosomes. *Mol. Biol. Cell* **22**, 375–385 (2011).
47. H. S. Saleh, U. Merkel, K. J. Geißler, T. Sperka, A. Sechi, C. Breithaupt, H. Morrison, Properties of an ezrin mutant defective in F-actin binding. *J. Mol. Biol.* **385**, 1015–1031 (2009).
48. S. Martinelli, E. J. H. Chen, F. Clarke, R. Lyck, S. Affentranger, J. K. Burkhardt, V. Niggli, Ezrin/radixin/moesin proteins and flotillins cooperate to promote uropod formation in T cells. *Front. Immunol.* **4**, 84 (2013).
49. S. Wälde, K. Thakar, S. Hutten, C. Spillner, A. Nath, U. Rothbauer, S. Wiemann, R. H. Kehlenbach, The nucleoporin Nup358/RanBP2 promotes nuclear import in a cargo- and transport receptor-specific manner. *Traffic* **13**, 218–233 (2012).

50. N. Yokoyama, N. Hayashi, T. Seki, N. Panté, T. Ohba, K. Nishii, K. Kuma, T. Hayashida, T. Miyata, U. Aebi, M. Fukui, T. Nishimoto, A giant nucleopore protein that binds Ran/TC4. *Nature* **376**, 184–188 (1995).
51. B. Cautain, R. Hill, N. de Pedro, W. Link, Components and regulation of nuclear transport processes. *FEBS J.* **282**, 445–462 (2015).
52. K. Huenniger, A. Krämer, M. Soom, I. Chang, M. Köhler, R. Depping, R. H. Kehlenbach, C. Kaether, Notch1 signaling is mediated by importins alpha 3, 4, and 7. *Cell. Mol. Life Sci.* **67**, 3187–3196 (2010).
53. N. Sachan, A. K. Mishra, M. Mutsuddi, A. Mukherjee, The *Drosophila* importin-α3 is required for nuclear import of notch in vivo and it displays synergistic effects with Notch receptor on cell proliferation. *PLOS ONE* **8**, e68247 (2013).
54. Y. Nam, P. Sliz, L. Song, J. C. Aster, S. C. Blacklow, Structural basis for cooperativity in recruitment of MAML coactivators to Notch transcription complexes. *Cell* **124**, 973–983 (2006).
55. P. Mittal, C. W. M. Roberts, The SWI/SNF complex in cancer—Biology, biomarkers and therapy. *Nat. Rev. Clin. Oncol.* **17**, 435–448 (2020).
56. Z. Pillidge, S. J. Bray, SWI/SNF chromatin remodeling controls Notch-responsive enhancer accessibility. *EMBO Rep.* **20**, e46944 (2019).
57. C. J. Fryer, E. Lamar, I. Turbachova, C. Kintner, K. A. Jones, Mastermind mediates chromatin-specific transcription and turnover of the notch enhancer complex. *Genes Dev.* **16**, 1397–1411 (2002).
58. C. J. Fryer, J. Brandon White, K. A. Jones, Mastermind recruits CycC:CDK8 to phosphorylate the Notch ICD and coordinate activation with turnover. *Mol. Cell* **16**, 509–520 (2004).
59. B. E. Housden, A. Q. Fu, A. Krejci, F. Bernard, B. Fischer, S. Tavaré, S. Russell, S. J. Bray, Transcriptional dynamics elicited by a short pulse of Notch activation involves feed-forward regulation by E(spl)/Hes genes. *PLOS Genet.* **9**, e1003162 (2013).
60. M. D. Rand, L. M. Grimm, S. Artavanis-Tsakonas, V. Patriub, S. C. Blacklow, J. Sklar, J. C. Aster, Calcium depletion dissociates and activates heterodimeric Notch receptors. *Mol. Cell. Biol.* **20**, 1825–1835 (2000).
61. J. Falo-Sanjuan, N. C. Lammers, H. G. Garcia, S. J. Bray, Enhancer priming enables fast and sustained transcriptional responses to Notch signaling. *Dev. Cell* **50**, 411–425.e8 (2019).
62. H. Park, F. V. Hundley, Q. Yu, K. A. Overmyer, D. R. Brademan, L. Serrano, J. A. Paulo, J. C. Paoli, S. Swarup, J. J. Coon, S. P. Gygi, J. Wade Harper, Spatial snapshots of amyloid precursor protein intramembrane processing via early endosome proteomics. *Nat. Commun.* **13**, 1–21 (2022).
63. H. Wang, C. Zang, L. Taing, K. L. Arnett, Y. J. Wong, W. S. Pear, S. C. Blacklow, X. S. Liu, J. C. Aster, NOTCH1-RBPJ complexes drive target gene expression through dynamic interactions with superenhancers. *Proc. Natl. Acad. Sci. U.S.A.* **111**, 705–710 (2014).
64. D. Castel, P. Mourikis, S. J. J. Bartels, A. B. Brinkman, S. Tajbakhsh, H. G. Stunnenberg, Dynamic binding of RBPJ is determined by Notch signaling status. *Genes Dev.* **27**, 1059–1071 (2013).
65. J. Falo-Sanjuan, S. J. Bray, Notch-dependent and -independent transcription are modulated by tissue movements at gastrulation. *eLife* **11**, e73656 (2022).
66. F. Oswald, B. Täuber, T. Dobner, S. Bourteele, U. Kostezka, G. Adler, S. Liptay, R. M. Schmid, p300 acts as a transcriptional coactivator for mammalian Notch-1. *Mol. Cell. Biol.* **21**, 7761–7774 (2001).
67. A. E. Wallberg, K. Pedersen, U. Lendahl, R. G. Roeder, p300 and PCAF act cooperatively to mediate transcriptional activation from chromatin templates by notch intracellular domains in vitro. *Mol. Cell. Biol.* **22**, 7812–7819 (2002).
68. M. Kalocsay, APEX peroxidase-catalyzed proximity labeling and multiplexed quantitative proteomics. *Methods Mol. Biol.* **2008**, 41–55 (2019).
69. J. Rappsilber, M. Mann, Y. Ishihama, Protocol for micro-purification, enrichment, pre-fractionation and storage of peptides for proteomics using StageTips. *Nat. Protoc.* **2**, 1896–1906 (2007).
70. G. C. McAlister, D. P. Nusinow, M. P. Jedrychowski, M. Wühr, E. L. Huttlin, B. K. Erickson, R. Rad, W. Haas, S. P. Gygi, MultiNotch MS3 enables accurate, sensitive, and multiplexed detection of differential expression across cancer cell line proteomes. *Anal. Chem.* **86**, 7150–7158 (2014).
71. J. K. Eng, A. L. McCormack, J. R. Yates, An approach to correlate tandem mass spectral data of peptides with amino acid sequences in a protein database. *J. Am. Soc. Mass Spectrom.* **5**, 976–989 (1994).
72. E. L. Huttlin, M. P. Jedrychowski, J. E. Elias, T. Goswami, R. Rad, S. A. Beausoleil, J. Villén, W. Haas, M. E. Sowa, S. P. Gygi, A tissue-specific atlas of mouse protein phosphorylation and expression. *Cell* **143**, 1174–1189 (2010).
73. J. A. Paulo, J. D. O'Connell, R. A. Everley, J. O'Brien, M. A. Gygi, S. P. Gygi, Quantitative mass spectrometry-based multiplexing compares the abundance of 5000 *S. cerevisiae* proteins across 10 carbon sources. *J. Proteomics* **148**, 85–93 (2016).
74. J. Schindelin, I. Arganda-Carreras, E. Frise, V. Kaynig, M. Longair, T. Pietzsch, S. Preibisch, C. Rueden, S. Saalfeld, B. Schmid, J. Y. Tinevez, D. J. White, V. Hartenstein, K. Eliceiri, P. Tomancak, A. Cardona, Fiji: An open-source platform for biological-image analysis. *Nat. Methods* **9**, 676–682 (2012).

Acknowledgments: We thank members of the Blacklow laboratory for helpful discussions. **Funding:** This work was supported by NIH awards 1R35 CA220340 (to S.C.B.) and 1R01 CA272484 (to S.C.B. and T.K.), 5R35 GM130386 (to T.K.), and K99 GM144750 (to J.M.R.). A.P.M. was supported by a Merck Postdoctoral Fellowship. L.T. was supported by Deutsche Forschungsgemeinschaft, WBP TV11/1. J.C.A. was supported by the Ludwig Center at Harvard. This work was conducted with support from the Cancer Prevention and Research Institute of Texas, grant RR220032 to M.K. This work was conducted with support from Harvard Catalyst | the Harvard Clinical and Translational Science Center (National Center for Advancing Translational Sciences, National Institutes of Health Award UL1 TR002541) and financial contributions from Harvard University and its affiliated academic healthcare centers. **Author contributions:** A.P.M. and S.C.B. conceived the project. S.C.B. and T.K. acquired funding. A.P.M. performed and analyzed experiments. E.D.E. performed initial characterization of the parental SVG-A cell line and designed and generated NOTCH2-HaloTag knockin and NOTCH2 knockout lines. G.A.B., R.J.E., and M.K. processed and analyzed MS data. L.T., G.S., and T.K. assisted with and gave technical advice for microscopy experiments. J.M.R., J.C.A., A.N.D., and M.K. assisted with data analysis and interpretation. A.P.M. and S.C.B. wrote the manuscript with input from all authors. All authors provided feedback and agreed on the final manuscript. **Competing interests:** S.C.B. is on the board of directors of the nonprofit Institute for Protein Innovation and the Revson Foundation; is on the scientific advisory board for and receives funding from Erasca Inc. for an unrelated project; is an adviser to MPM Capital; and is a consultant for IFM, Scorpion Therapeutics, Odyssey Therapeutics, Droia Ventures, and Ayala Pharmaceuticals for unrelated projects. J.C.A. is a consultant for Ayala Pharmaceuticals, Cellestia Inc., SpringWorks Therapeutics, and Remix Therapeutics. The other authors declare that they have no competing interests. **Data and materials availability:** Proteomics raw data and search results were deposited in the PRIDE archive (https://ebi.ac.uk/pride/archive/) for each multiplex experiment with accession numbers PXD039008 (immobilized ligand with GSI experiment), PXD042123 (both the broad and early coculture with JAG1-expressing A673 cell experiments), and PXD039010 (immobilized ligand with GSI nuclear-centered experiment). All other data needed to evaluate the conclusions in the paper are present in the paper or the Supplementary Materials.

Submitted 11 January 2023
Resubmitted 10 April 2023
Accepted 7 July 2023
Published 1 August 2023
10.1126/scisignal.adg6474

Science Signaling

A spatiotemporal Notch interaction map from plasma membrane to nucleus

Alexandre P. Martin, Gary A. Bradshaw, Robyn J. Eisert, Emily D. Egan, Lena Tveriakhina, Julia M. Rogers, Andrew N. Dates, Gustavo Scanavachi, Jon C. Aster, Tom Kirchhausen, Marian Kalocsay, and Stephen C. Blacklow

Sci. Signal., **16** (796), eadg6474.
DOI: 10.1126/scisignal.adg6474

Science Signaling (ISSN) is published by the American Association for the Advancement of Science. 1200 New York Avenue NW, Washington, DC 20005. The title *Science Signaling* is a registered trademark of AAAS.